CALL FOR PAPERS | *Renal hemodynamics: integrating with the nephron and beyond*

# Dominant factors that govern pressure natriuresis in diuresis and antidiuresis: a mathematical model

**Robert Moss[1,2] and Anita T. Layton[1]**

[1]*Department of Mathematics, Duke University, Durham, North Carolina; and* [2]*The Melbourne School of Population and Global Health, University of Melbourne, Melbourne, Australia*

Moss R, Layton AT. Dominant factors that govern pressure natriuresis in diuresis and antidiuresis: a mathematical model. *Am J Physiol Renal Physiol* 306: F952–F969, 2014. First published February 19, 2014; doi:10.1152/ajprenal.00500.2013.—We have developed a whole kidney model of the urine concentrating mechanism and renal autoregulation. The model represents the tubuloglomerular feedback (TGF) and myogenic mechanisms, which together affect the resistance of the afferent arteriole and thus glomerular filtration rate. TGF is activated by fluctuations in macula densa [Cl⁻] and the myogefnic mechanism by changes in hydrostatic pressure. The model was used to investigate the relative contributions of medullary blood flow autoregulation and inhibition of transport in the proximal convoluted tubule to pressure natriuresis in both diuresis and antidiuresis. The model predicts that medullary blood flow autoregulation, which only affects the interstitial solute composition in the model, has negligible influence on the rate of NaCl excretion. However, it exerts a significant effect on urine flow, particularly in the antidiuretic kidney. This suggests that interstitial washout has significant implications for the maintenance of hydration status but little direct bearing on salt excretion, and that medullary blood flow may only play a signaling role for stimulating a pressure-natriuresis response. Inhibited reabsorption in the model proximal convoluted tubule is capable of driving pressure natriuresis when the known actions of vasopressin on the collecting duct epithelium are taken into account.

kidney; salt excretion; autoregulation; medullary blood flow; urine concentration

ACUTE ELEVATION OF RENAL PERFUSION pressure produces large increases in NaCl excretion in volume-expanded animals (1, 16, 45, 63, 84). Antidiuretic animals exhibit a similar response but with a significantly diminished magnitude (33, 34, 82). Natriuresis can also occur without elevations in renal perfusion pressure (9, 10, 25).

A substantial body of evidence suggests that pressure natriuresis is driven, at least in part, by elevated renal interstitial hydrostatic pressure (RIHP) (22, 36, 37). Increased RIHP is linked to elevated medullary blood flow (MBF), which is in turn modulated by vasopressin (23). This may explain why the magnitude of the pressure natriuresis depends on hydration status. However, the mechanisms that cause salt excretion to be sensitive to RIHP and MBF remain insufficiently well characterized.

Renal decapsulation reduces RIHP and significantly diminishes (but does not eliminate) pressure natriuresis (34, 37, 44, 48). Experimental evidence suggests that MBF has a negligible direct effect on salt and water reabsorption in the loop of Henle and the collecting duct (CD) (21, 28, 85). Instead, it has been proposed that elevated MBF initiates signals that mediate pressure-natriuretic responses (21). This signaling cascade includes the inhibition of sodium reabsorption in the proximal convoluted tubule (PCT) (67, 79). This inhibition can be partially countered by infusion of angiotensin II (62, 66, 103). Here we restrict our consideration to the direct effects of elevated MBF on the medullary interstitium (and, therefore, on reabsorption in the loop of Henle, the vasa recta, and the CD) and of inhibited sodium reabsorption in the PCT.
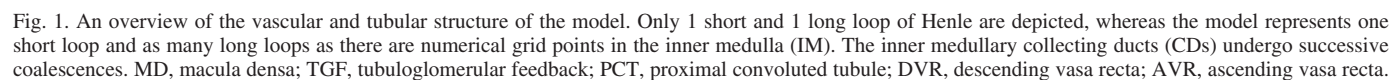
Both elevated MBF and inhibited PCT sodium reabsorption can affect urine flow and NaCl concentration. It remains unclear whether the direct effects of MBF on the interstitium are entirely irrelevant to the pressure natriuresis response and whether the inhibition of NaCl reabsorption in the PCT is sufficient to elevate NaCl excretion to levels observed in volume-expanded animals. To date, there is no experimental technique that allows MBF to be controlled independently of hydration status, meaning that experimental investigations cannot easily address this question. Furthermore, a recent study of a detailed whole kidney model highlighted the importance of the pressure-sensitive inhibition of PCT sodium reabsorption for predicting whole kidney water and NaCl excretion rates but provided only a cursory treatment of the matter (68).

We present a mathematical model of water and NaCl excretion that can independently regulate MBF, glomerular filtration, and proximal tubule NaCl reabsorption. By studying how model excretion rates are affected by MBF and PCT reabsorption, we identify the key factors responsible for driving pressure natriuresis in the model. We show that the model can reproduce acute renal function curves measured in both antidiuretic and volume-expanded rats. We then evaluate whether the differences in model parameters between the antidiuretic and volume-expanded cases offer a plausible explanation for the different magnitudes of pressure natriuresis that are observed in vivo in volume-expanded and volume-depleted animals.

## METHODS

The model comprises an existing medullary model of the urine concentrating mechanism that encompasses the tubular and vascular architecture of both the outer and inner medulla (55), a glomerular model that encompasses the afferent and efferent arterioles and the glomerular capillary bed, a model of the myogenic and tubuloglomerular feedback (TGF) responses that regulate afferent blood flow, a PCT segment that exhibits pressure-dependent reabsorption of the filtered load, and a cortical thick ascending limb (cTAL) segment that predicts macula densa delivery, providing the input signal for the TGF response. The model structure is shown in Fig. 1.

Fig. 1. An overview of the vascular and tubular structure of the model. Only 1 short and 1 long loop of Henle are depicted, whereas the model represents one short loop and as many long loops as there are numerical grid points in the inner medulla (IM). The inner medullary collecting ducts (CDs) undergo successive coalescences. MD, macula densa; TGF, tubuloglomerular feedback; PCT, proximal convoluted tubule; DVR, descending vasa recta; AVR, ascending vasa recta.

*Renal blood flow and glomerular filtration.* The glomerular model comprises the afferent and efferent arterioles and a glomerular capillary bed. The net pressure drop across the vasculature is determined by the renal perfusion pressure ($P_{RPP}$) and the venous return pressure ($P_v = 3.75$ mmHg). Afferent arteriolar resistance ($R_{Aff}$) is determined by the combined activation of the TGF and myogenic responses, based on the model of Feldberg et al. (30). The activation of these responses varies along the length of the afferent arteriole, where $x = 0$ is the start of the arteriole and $x = 1$ is the entry to the glomerulus. The model represents TGF as a sigmoidal response (shown in Fig. 2) whose activation ($\Psi_{TGF}$) is determined by the macula densa $Cl^-$ concentration ($C_{Cl}$, mM) and the TGF-operating point ($C_{Op}$, mM):

$$\Psi_{TGF}(1) = \Psi_{MAX} + \frac{\Psi_{MIN} - \Psi_{MAX}}{1 + e^{K_{TGF}(C_{Cl} - C_{Op})}} \quad (1)$$

This activation is assumed to decrease linearly with increasing distance from the glomerulus ($x = 1$), disappearing at $x = 0.9$:

$$\Psi_{TGF}(x) = \begin{cases} \Psi_{TGF}(1) \cdot (10x - 9) & \text{when } x \geq 0.9 \\ 0 & \text{otherwise} \end{cases} \quad (2)$$

Experimental data suggest that the relationship between transmural pressure (across the afferent arteriole wall) and the activation of the myogenic response is nearly linear (30). Accordingly, we assume the activation of the myogenic response ($\Psi_{MYO}$) is a linear function of the transmural pressure ($P$):

$$\Psi_{MYO}(P) = \begin{cases} 0 & \text{for } P < P_{MIN} \\ \dfrac{P - P_{MIN}}{P_{MAX} - P_{MIN}} & \text{for } P_{MIN} \leq P \leq P_{MAX} \\ 1 & \text{for } P_{MAX} < P \end{cases} \quad (3)$$

The values of $P_{MIN}$ and $P_{MAX}$ were derived from experimental measurements (26). The net activation of the smooth muscle is assumed to be the sum of the two responses:

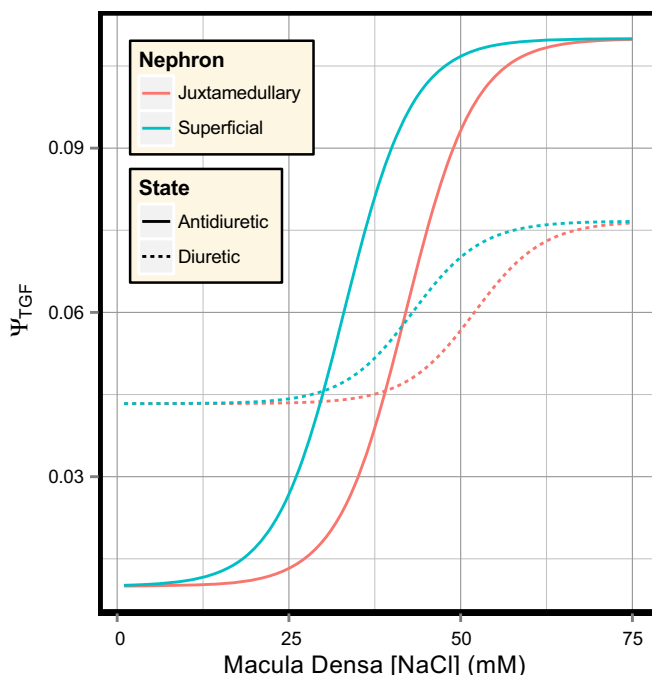$$\Psi(x) = \Psi_{TGF}(x) + \Psi_{MYO}(x) \quad (4)$$



Fig. 2. TGF response for the superficial and juxtamedullary nephrons.

By treating the wall of the afferent arteriole as rings of smooth muscle and applying Laplace's law (as per Feldberg et al. 30), the transmural pressure $P$ can be written in the form:

$$P = \int_1^\eta \frac{\sigma}{\sqrt{r_p^2 - 1 + z^2}} dz \; ; \; r_p = \frac{r_i}{\rho_i} \; ; \; \eta = \frac{\rho_o}{\rho_i} \quad (5)$$

where $\rho_i$ and $\rho_o$ are the inner and outer radii of the vessel wall when the transmural pressure $P = 0$, $r_i$ and $r_o$ are the inner and outer radii of the vessel wall for the transmural pressure $P$, and $\sigma$ is the idealized stress of the vascular smooth muscle. This stress comprises passive stress ($\sigma_e$) due to the elastic elements of the wall and active stress ($\sigma_a$) due to the contraction of the vascular smooth muscle:

$$\sigma = \sigma_e + \Psi \sigma_a \quad (6)$$

$$\sigma_e = C_1(e^{\alpha_1 \varepsilon} - 1) + C_2(e^{\alpha_2 \varepsilon} - 1) \quad (7)$$

$$\sigma_a = \begin{cases} \sigma_{MAX}\left(1 - \left|\dfrac{\varepsilon - \varepsilon_{MAX}}{\varepsilon_w}\right|\right) & \text{for } |\varepsilon - \varepsilon_{MAX}| < \varepsilon_w \\ 0 & \text{otherwise} \end{cases} \quad (8)$$

$$\varepsilon = \frac{1}{z}\sqrt{r_p^2 - 1 + z^2} - 1 \quad (9)$$

where $C_1$, $C_2$, $\alpha_1$, $\alpha_2$ are constants, estimated experimentally (20). The common strain $\varepsilon$ represents the shortening or lengthening of the elastic and collagen fibers in the vessel wall, and $\varepsilon_w$ is the working range of the overlap between the myosin and actin filaments (30).

We model the afferent arteriole as a sequence of $n = 100$ vascular smooth muscle segments. The resistance of each segment ($R_j$) was approximated using Poiseuille's law and the inner radius of the segment ($r_i$):

$$R_j = \frac{k}{r_i^4 \cdot n} \quad (10)$$

where $k$ is a constant that depends on blood viscosity and $n$ is the number of segments. The transmural pressure at the mid-point of each segment was approximated by distributing the pressure drop across the afferent arteriole in proportion to each segment resistance:

$$R_{Aff} = \sum_{m=1}^n R_m \quad (11)$$

$$P_0 = \frac{2}{3}P_{RPP} \quad (12)$$

$$P_j = P_0 - [P_0 - P_G(0)]\frac{0.5R_j + \sum_{m=1}^{j-1} R_m}{R_{Aff}} \quad (13)$$

where $P_0$ and $P_G(0)$ are the hydrostatic pressures at the beginning and end of the arteriole. The initial hydrostatic pressure was defined on the basis that the afferent arteriole is preceded by several levels of renal vasculature. The regulatory range of the model myogenic response is $65 \leq P_0 \leq 120$ mmHg. By assuming that the renal perfusion pressure (RPP) is reduced by one-third before reaching the afferent arteriole, the myogenic response provides efficient autoregulation of renal blood flow (RBF) for $100 \leq 180$ mmHg. This autoregulatory range is consistent with experimental measurements of glomerular filtration rate (GFR) and RBF. The afferent blood flow is determined by the net afferent resistance and the pressure drop across the arteriole:

$$B_{Aff} = \frac{P_0 - P_G(0)}{R_{Aff}} \quad (14)$$

The single-nephron glomerular filtration rate (SNGFR) and efferent blood flow are then calculated by integrating flow and pressure equations along the glomerular capillary bed ($0 \leq x \leq 1$):

$$Q_{\text{Aff}} = B_{\text{Aff}} \times (1 - h) \tag{15}$$

$$B_G(x) = B_{\text{Aff}} - \int_0^x K_f[P_G(x) - \Pi(x) - P_{\text{BS}}]dx \tag{16}$$

$$Q_G(x) = Q_{\text{Aff}} - \int_0^x K_f[P_G(x) - \Pi(x) - P_{\text{BS}}]dx \tag{17}$$

$$P_G(x) = P_G(0) - \int_0^x R_G B_G(x)dx \tag{18}$$

$$\Pi(x) = 2.1 \cdot C_{\text{Pr}}(x) + 0.16 \cdot C_{\text{Pr}}(x)^2 + 0.009 \cdot C_{\text{Pr}}(x)^3 \tag{19}$$

$$C_{\text{Pr}}(x) = C_{\text{Pr}}(0) \cdot \frac{Q_{\text{Aff}}}{Q_G(x)} \tag{20}$$

$$B_{\text{Eff}} = B_G(1) \tag{21}$$

$$P_{\text{Eff}} = P_G(1) \tag{22}$$

To solve these equations and determine the renal blood flow and GFR, the inner radius of each afferent arteriole segment and the initial glomerular pressure $P_G(0)$ must be determined. This is achieved with an iterative scheme. Initially, the radius of each segment is set to $\rho_i$. The resistance of each segment and of the entire arteriole are calculated *Eqs. 10* and *11*. $P_G(0)$ is then approximated iteratively such that solving *Eqs. 14–22* satisfies:

$$\left| P_G(1) - B_{\text{Eff}} R_{\text{Eff}} - P_V \right| \leq 10^{-3} \tag{23}$$

The hydrostatic pressure profile along the afferent arteriole can then be calculated using (13). The myogenic activation $\Psi_{\text{MYO}}(x)$ is then updated and the inner radius of each segment is calculated to satisfy (5). These steps are repeated until the relative change in radius per iteration is $<10^{-8}$ for every segment.

*Medullary model.* The medullary portion of the model is based on a model that has previously been used to investigate the role that the vascular architecture in the inner medulla (IM) plays in the process of urine concentration (55). The model incorporates recent experimental findings on the relative positions of the tubules and vasa recta, as well as their transport properties (49, 73, 104), and explicitly represents short and long loops of Henle, ascending and descending vasa recta,
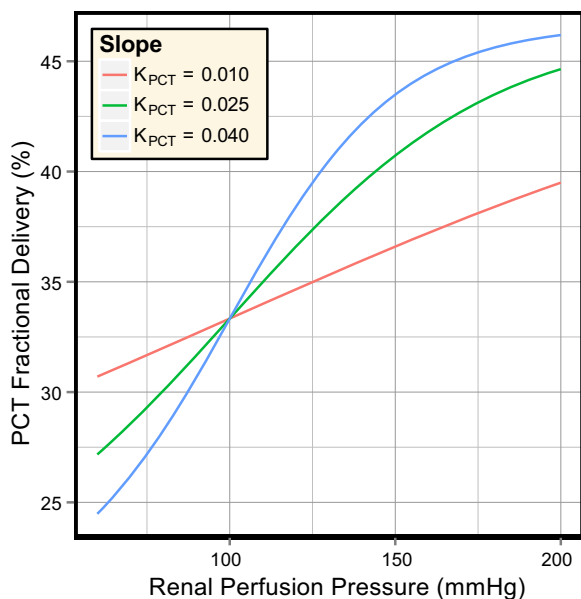


Fig. 3. Fractional delivery in the PCT segment for several values of the slope ($K_{\text{PCT}}$), shown for the range of perfusion pressures used in the model simulations.

**Table 1. cTAL parameters for each nephron**

| Parameter | Superficial | | Juxtamedullary |
|---|---|---|---|
| $L_{\text{cTAL}}$ | 3 mm | | 1 mm |
| Radius | | 10 µm | |
| $P_f$ | | 0 cm/s | |
| $P_{\text{Na}}$ | | $1 \times 10^{-5}$ cm/s | |
| $P_{\text{Ur}}$ | | $0.5 \times 10^{-5}$ cm/s | |
| $K_m$ | | 70 mM | |
| $V_{\text{max}}$ | 12.5 nmol/cm$^2$s | | 25.9 nmol/cm$^2$s |

cTAL, cortical thick ascending limb; see text for additional definitions.

and a composite CD. Short loops turn at the outer medulla (OM)-IM boundary, while long loops turn at every depth of the IM. Model descending vasa recta (DVR) terminate at every depth of the entire medulla. The model encompasses three solutes: NaCl, urea, and a nonreabsorbable solute that represents all solutes that are neither reabsorbed nor secreted along the nephron tubule and CD. The model predicts fluid flow, solute concentrations, and transepithelial fluxes along each tubule and vessel at every depth of the medulla, and the interstitial solute concentrations for each region. Parameter values for the medullary model can be found in Layton et al. (55).

*Cortical tubule segments and delivery to the collecting duct.* The model admits three cortical tubule segments. Reabsorption in the proximal and distal convoluted tubules is controlled by fractional delivery coefficients. The cTAL is represented as an explicit epithelium and is used to determine the macula densa NaCl concentration.

Fractional delivery of NaCl (and, therefore, water) from the PCT to the proximal straight tubule (PST) is a sigmoidal function of the renal perfusion pressure, as defined by *Eqs. 24* and *25* and shown in Fig. 3. When $R_{\text{RPP}} = 100$ mmHg the PCT fractional delivery is 1/3.

$$FD_{\text{PCT}} = K_1 - (K_1 - K_0) \cdot \frac{1}{1 + e^{K_{\text{PCT}}(P_{\text{RPP}} - K_{\text{Op}})}} \tag{24}$$

$$F_{\text{PST}}(0) = (Q_{\text{Aff}} - Q_{\text{Eff}}) \times FD_{\text{PCT}} \tag{25}$$

The cortical ascending limbs are represented as explicit epithelia (parameter values are listed in Table 1), and the macula densa NaCl concentration is assumed to be that of the cTAL outflow. The epithelial properties of this segment are identical to those of the outer-medullary ascending limb. The segment is 3-mm long for superficial nephrons and 1-mm long for juxtamedullary nephrons.

The outer medullary collecting duct (OMCD) delivery is calculated from the outflow of the cortical thick ascending limbs (i.e., the flow at the macula densa) of each nephron (26). The fractional delivery coefficients are listed in Table 2, and the urea concentration is calculated such that the fluid entering the OMCD is isosmotic to blood plasma (307 mosmol/kgH$_2$O). The delivery to a single OMCD is weighted by the ratio of superficial to juxtamedullary nephrons and scaled to respect the 6.1:1 ratio of nephrons to CDs (51):

**Table 2. Hydration-dependent parameter values**

| Parameter | Antidiuretic | Diuretic |
|---|---|---|
| $\Psi_{\text{MIN}}$ | 0.01 | 0.0433 |
| $\Psi_{\text{MAX}}$ | 0.11 | 0.0767 |
| $C_{\text{Op}}$ (superficial) | 33 mM | 43 mM |
| $C_{\text{Op}}$ (juxtamedullary) | 42 mM | 52 mM |
| $FD_{\text{DCT}}(V)$ | 16.5% | 36.4% |
| $FD_{\text{DCT}}(\text{Na})$ | 11.0% | 32.2% |
| OMCD $P_f$ | $463 \times 10^{-5}$ cm/s | $23.15 \times 10^{-5}$ cm/s |
| IMCD$(x)$ $P_f$ | $750 \times 10^{-4}$ cm/s | $(6 - 3.5 \cdot x/L)^{-1} \cdot$ $750 \times 10^{-4}$ cm/s |
| IMCD $P_{\text{Ur}}$ | $110 \times 10^{-5}$ cm/s | $46 \times 10^{-5}$ cm/s |

OMCD, outer medullary collecting duct; IMCD, inner medullary collecting duct; see text for additional definitions.

Table 3. *Glomerular parameters*

| Parameter | Units | Value |
|---|---|---|
| $\rho_o$ | $\mu$m | 13 $\searrow$ 11.7 |
| $\rho_i$ | $\mu$m | 10 $\searrow$ 9 |
| $h$ | — | 0.45 |
| $K_f$ | nl·min$^{-1}$·mmHg$^{-1}$ | 1.6*/1.9† |
| $K_{TGF}$ | mM$^{-1}$ | 0.2 |
| $P_{BS}$ | mmHg | 15 |
| $P_V$ | mmHg | 3.75 |
| $R_{Eff}$ | mmHg·min·nl$^{-1}$ | 0.4 |
| $R_G$ | mmHg·min·nl$^{-1}$ | 0.001 |
| $K_0$ | — | 3/15 |
| $K_1$ | — | 7/15 |
| $K_{Op}$ | mmHg | 100 |
| $P_{MIN}$ | mmHg | 42.3 |
| $P_{MAX}$ | mmHg | 86.7 |
| $C_1$ | mmHg | 20.25 |
| $\alpha_1$ | — | 2.0 |
| $C_2$ | mmHg | 1.88 |
| $\alpha_2$ | — | 12.0 |
| $\sigma_{MAX}$ | mmHg | 750 |
| $\epsilon_{MAX}$ | — | 0.25 |
| $\epsilon_w$ | — | 0.9 |
| $k$ | mmHg·min·$\mu$m | 9.406 |
| $n$ | — | 100 |

$\searrow$, Decreases linearly. See text for other definitions. *Superficial; †juxtamedullary.

$$F_{OMCD}(0) = 6.1 \times F_{cTAL}(L_{cTAL}) \times FD_{DCT} \qquad (26)$$

The DVR inflow has a reference value of 8 nl/min (as per the original boundary conditions; Ref. 55) and varies as a linear function of renal perfusion pressure:

$$F_{DVR}(0) = 8 \text{ nl/min} + K_{MBF}(P_{RPP} - 100) \qquad (27)$$

*Hydration status and epithelial properties.* Model parameters from Ref. 55 are used to predict water and salt excretion in antidiuresis. To simulate diuresis, we adjusted the epithelial properties of the CD and the fractional reabsorption parameters for the distal convoluted tubule (DCT) to reflect the change in hydration status. The antidiuretic hormone (ADH) concentration is assumed to decrease sufficiently that the CD water permeability and inner medullary collecting duct (IMCD) urea permeability are minimal (see Table 2).

The DCT fractional reabsorption coefficients were adjusted so that the OMCD inflow was increased from 6.5 to 15.0 nl/min (per individual OMCD), assuming the DCT tubular fluid/plasma ratio inulin ratio is ~9 (2) and that no water reabsorption occurs along the cortical collecting duct. Water permeabilities of the OMCD, initial IMCD, and terminal IMCD were reduced by factors of 20, 6, and 2.5,

respectively (89), and urea permeability of the terminal IMCD was reduced from $110 \times 10^{-5}$ to $46 \times 10^{-5}$ cm/s (89).

The TGF gain was also reduced by a factor of 3 in the diuretic model, and the TGF operating points for the superficial and juxtaglomerular nephrons were increased by 10 mM (Table 2). The other glomerular parameters are not hydration-dependent (see Table 3).

*Regulation of water and salt excretion.* The parameters of interest for exploring how the model regulates water and salt excretion, with regards to renal perfusion pressure, are the slopes of the MBF autoregulatory curve and the pressure-sensitive inhibition of sodium reabsorption in the PCT (hereafter referred to as the "PCT response"):

$K_{MBF}$: MBF is well-regulated in antidiuretic rats and poorly regulated in volume expanded rats. ADH presumably plays a significant role since it varies in response to hydration status and has a vasoconstrictive effect on the DVR. If $K_{MBF} = 0$, MBF (see *Eq. 27*) is perfectly autoregulated. As $K_{MBF}$ increases, MBF autoregulation decreases.

$K_{PCT}$: the response is amplified in volume-expanded rats and diminished in antidiuretic rats and is believed to be mediated (at least in part) by the medullary interstitial hydrostatic pressure (which may be sensitive to ADH). Angiotensin II also has an significant effect on PCT reabsorption. The value of $K_{PCT}$ (see *Eq. 24*) is the maximal slope of the response.

In particular, the interaction between these two mechanisms and the combined effect they exert on NaCl excretion are the critical determinants of the pressure-natriuresis response of the model.

## RESULTS

Adult rats are consistently observed to have GFRs of around 1.0 ml·min$^{-1}$·g kidney weight$^{-1}$ (kwt) and whole body GFRs in the range of 2.3–3.0 ml/min (Table 4). Within the autoregulatory range, the model whole body GFR is 2.43 ml/min (assuming that a rat kidney contains 38,000 nephrons; Ref. 99), suggesting the model "single kidney weight" is 1.2 g kwt. To report solute and volume excretion rates in units consistent with experimental studies ($\mu$eq·min$^{-1}$·g kwt$^{-1}$ and $\mu$l·min$^{-1}$·g kwt$^{-1}$, respectively), the IMCD volume and solute outflow rates were scaled by 38,000/(1.2·6.1) under the assumptions that a rat kidney contains 38,000 nephrons (99), that the model represents a single kidney of 1.2 g kwt, and that the ratio of nephrons to individual CDs in the model is 6.1:1 (51, 55).

Volume and solute transport along portions of individual tubule segments are reported with respect to the medullary depth, where 0 mm refers to the corticomedullary boundary and 7 mm to the papillary tip. Cortical segments are reported with negative depths, from the corticomedullary boundary

Table 4. *Comparison of the antidiuretic model to in vivo measurements of whole body GFR in the rat*

| | Weight, g | GFR, ml·min$^{-1}$·g kwt$^{-1}$ | Kidneys, g | GFR, ml/min |
|---|---|---|---|---|
| Model (32 $\times$ 10$^3$ nephrons) (8) | | | $\approx$2.05* | 2.05 |
| Model (38 $\times$ 10$^3$ nephrons (99) | | | $\approx$2.43* | 2.43 |
| Sprague-Dawley (male) (81) | | 1.0 | 2.54 | 2.54 |
| Sprague-Dawley (male) (79) | 225–300 | 1.03 | 2.92 | 3.01 |
| Dahl (female) (83) | 235 | 1.0 | 2.30 | 2.30 |
| Sprague-Dawley (male) (38) | 150 | 1.2 | | |
| Sprague-Dawley (male) (56) | | 0.9 | | |
| Sprague-Dawley (male) (58) | | 1.0–1.2 | | |
| Munich-Wistar (60) | 200–250 | 1.2 | | |
| Charles River (male, hydropenic) (7) | 320–350 | | | 3.00 |
| Sprague-Dawley (male) (103) | 170–230 | | | 1.0–1.4 |

Evaluated within the autoregulatory range of the model, where *n* is the assumed number of nephrons in a single rat kidney; g kwt, kidney weight in grams. Numbers in parenthesis indicate reference numbers. *Calculated by assuming glomerular filtration rate (GFR) $\approx$ 1.0 ml·min$^{-1}$·g kwt$^{-1}$.

(0 mm) to macula densa (−1 and −3 mm for the juxtamedullary and superficial cTAL, respectively).

*Base case (antidiuresis).* Water and solute flows in the longest loop of Henle, vasa recta, CD, and aggregate superficial/juxtamedullary cTAL segments are shown in Fig. 4. Solute concentrations and osmolalities are shown in Fig. 5. Urine flow and composition are summarized in Table 5. The vast majority of water reabsorption in the descending limbs occurs in the OM. Together the ascending limb segments reabsorb one-half of the NaCl load, the bulk of which is reabsorbed in the OM. Net reabsorption (5–7 mm) and net secretion (2–5 mm) of NaCl both occur along the IM ascending thin limbs.

Water is rapidly reabsorbed from the CD in the outer stripe. It is then reabsorbed at an approximately linear rate in the inner

stripe and upper IM (0.4–4.5 mm). In the deep IM (5–7 mm), CD water reabsorption is enhanced due to the high IMCD urea permeability, and the bulk of the IMCD urea load is reabsorbed into the interstitium. In contrast, there is a small amount of NaCl secretion into the OMCD (where the thick limb active transport of NaCl is highest) and the bulk of the CD NaCl reabsorption occurs in the upper IMCD.

*Base case (diuresis).* Key results for a diuretic kidney are shown in Figs. 4 and Fig. 5. Compared with the antidiuretic model, the descending limb of Henle and DVR inflow rates are unchanged and there is a similar degree of water reabsorption in the outer medullary descending limb segments. However, pronounced water secretion into the descending limbs in the IM increases the ascending limb water flow rates. In the IM there is significant NaCl secretion into the ascending limb of
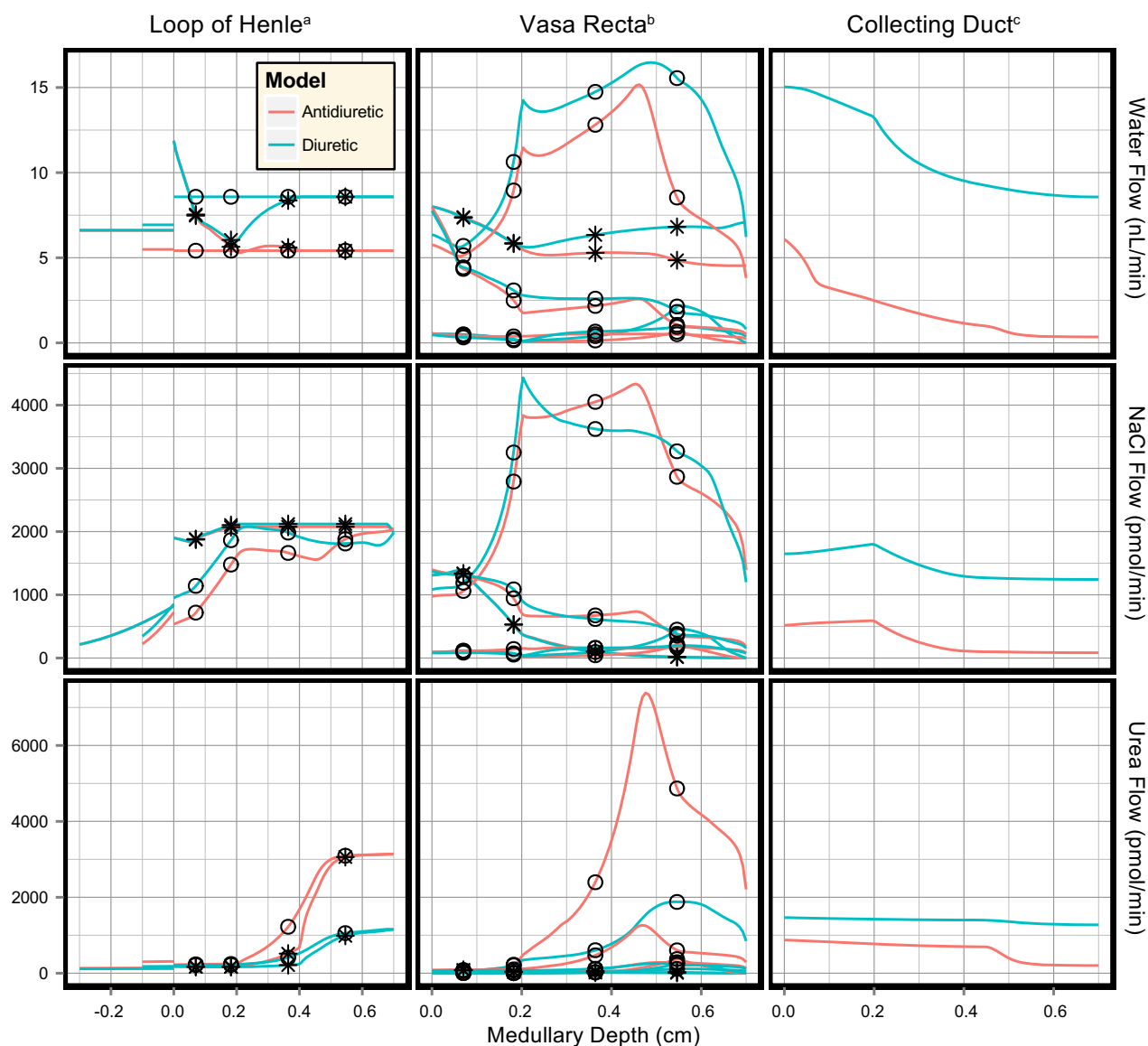


Fig. 4. Water and solute flow in the antidiuretic and diuretic models ($P_{RPP}$ = 100 mmHg). Profiles are shown for the longest loop of Henle and longest vasa recta. Negative depths depict the cortical thick ascending limb (cTAL) segments of the superficial nephron (3 mm in length) and the aggregate juxtamedullary nephron population (1 mm in length). The cTAL profiles are discontinuous at $x = 0$ since they contain the aggregate flow of all superficial and juxtamedullary nephrons, respectively. ○Flow profiles in ascending limbs of Henle and AVR. *Flow profiles in descending limbs of Henle and DVR. [a]Loop of Henle flow is shown per nephron. [b]Vasa recta flow is shown per individual DVR. [c]CD flow is shown per individual CD (6.1 nephrons).
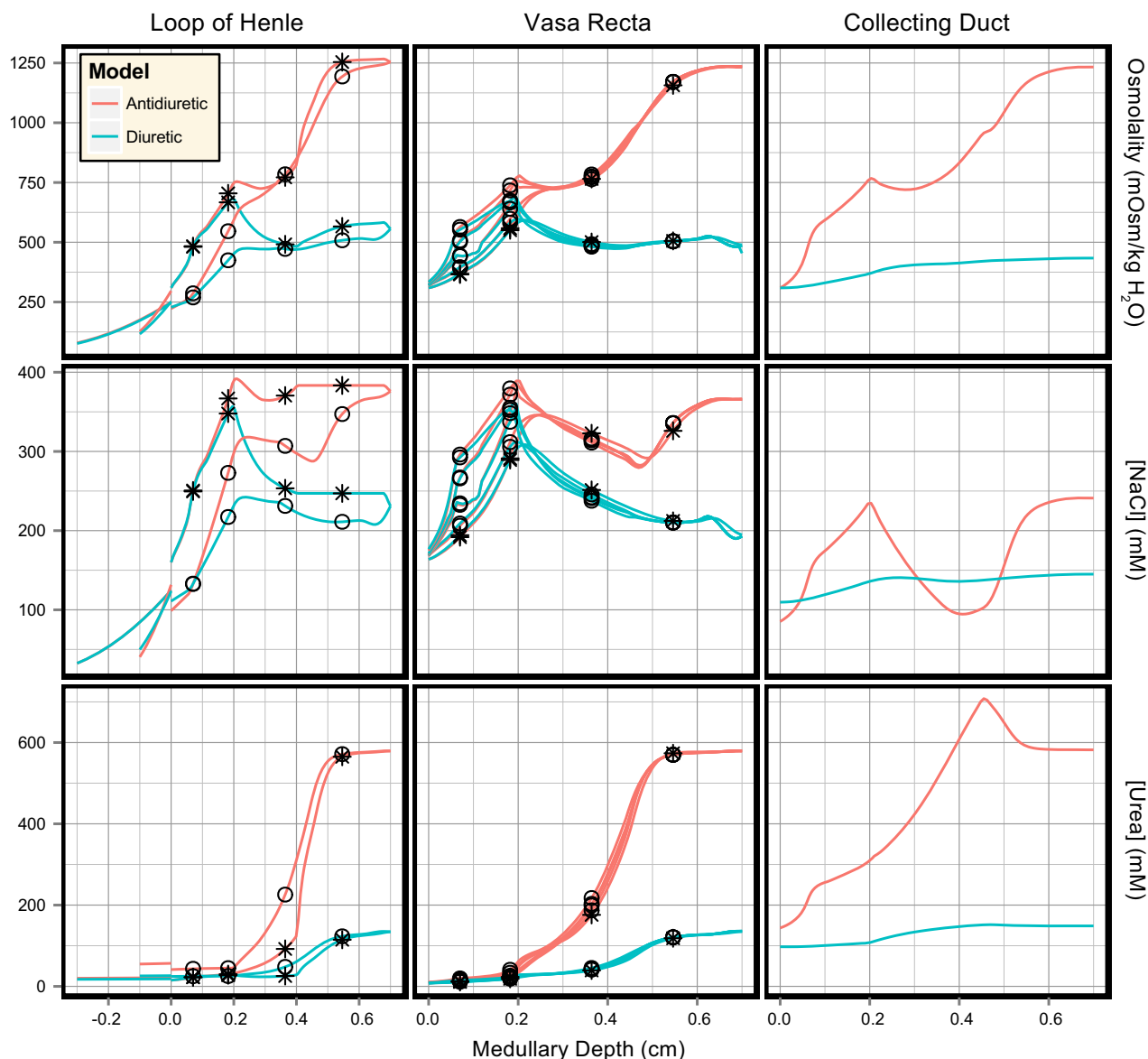
Fig. 5. Solute concentration and osmolality profiles in the antidiuretic and diuretic models ($P_{RPP} = 100$ mmHg). Profiles are shown as per Fig. 4. ○Concentration profiles in ascending limbs of Henle and AVR. *Concentration profiles in descending limbs of Henle and DVR.

Henle, which enhances NaCl delivery to the OM and the cTAL segments. There is also significant water secretion into the DVR in the IM, resulting in papillary DVR flow rates 50% higher than in the antidiuretic model.

Table 5. *Comparison of the model urine in antidiuretic and diuretic states when the perfusion pressure $P_{RPP} = 100$ mmHg*

| Quantity | Antidiuretic | Diuretic |
|---|---|---|
| Flow rate, nl·min$^{-1}$·CD | 0.35 | 8.57 |
| Flow rate, ul·min$^{-1}$·g kwt$^{-1}$ | 1.82 | 44.49 |
| Osmolality, mosmol/kgH$_2$O | 1233 | 434 |
| [NaCl], mM | 241 | 145 |
| [Urea], mM | 582 | 149 |
| NaCl excretion, ueq·min$^{-1}$·g kwt$^{-1}$ | 0.44 | 6.45 |
| Urea excretion, ueq·min$^{-1}$·g kwt$^{-1}$ | 1.05 | 6.62 |

CD, collecting duct.

Volume delivery to the OMCD in the diuretic model is assumed to be elevated in the diuretic model (6.1 vs. 15.0 nl/min). This results in a much larger load on the urine concentrating mechanism. Combined with the diminished CD water permeability, CD volume reabsorption is greatly reduced. CD fractional water reabsorption decreased from 94 to 43% in the diuretic model. Increased OMCD delivery and diminished CD water reabsorption result in higher NaCl and urea flow rates along the entirety of the CD, although the profiles for both solutes are similar in shape to those observed in the antidiuretic model. Urea reabsorption in the terminal IMCD is diminished due to the lowered IMCD urea permeability, reducing the quantity of urea available for recycling in the IM. CD fractional reabsorption of both NaCl and urea are significantly decreased in the diuretic model, from 84 to 25% (NaCl) and 77 to 13% (urea), even though the absolute water and NaCl reabsorption rates are slightly higher in the diuretic model.

The increased OMCD delivery, decreased urea recycling, and decreased water reabsorption along the medullary CD produce a 25-fold increase in urine flow rate, a 65% decrease in urine osmolality, a 15-fold increase in NaCl excretion, and a 6.3-fold increase in urea excretion, relative to the antidiuretic model (summarized in Table 5).

*Medullary blood flow autoregulation in antidiuresis.* Simulations were conducted for several values of $K_{MBF}$, 0, 0.005, 0.010, and 0.015 nl·min$^{-1}$·mmHg$^{-1}$ to determine the sensitivity of the model excretion rates to MBF. For each simulation, the PCT response was fixed ($K_{PCT} = 0.025$) and renal perfusion pressure was incremented from 76 to 194 mmHg. Model SNGFR was well regulated except for $P_{RPP} \leq 90$ mmHg, where it was significantly diminished. Superficial SNGFR was otherwise maintained between 29 and 33 nl/min and juxtamedullary SNGFR between 35 and 39 nl/min. The urine volume, osmolality and solute concentrations produced by the model for each value of $K_{MBF}$ are shown in Fig. 6.

Urine flow rate and solute excretion rates increased in proportion to the slope of the MBF curve ($K_{MBF}$), while urine osmolality exhibited an inverse relationship to $K_{MBF}$. When renal perfusion pressure was increased from 100 to 200 mmHg, urine flow rate increased by 9–15-fold (depending on $K_{MBF}$), urine osmolality decreased by 50–64%, NaCl excretion increased by 620–660%, and urea excretion increased by 400–

560%. Urine flow rate, osmolality, and urea excretion rate are all sensitive to $K_{MBF}$. In contrast, NaCl excretion exhibits almost complete insensitivity to $K_{MBF}$ and varied by only 7% at $P_{RPP} = 200$ mmHg.

Two benchmark values of $K_{MBF}$, 0 and 0.0125, correspond to perfect autoregulation as observed in volume-depleted rats and to weak autoregulation as observed in volume-expanded rats (33, 65). A comparison of flow and solute concentration profiles for these benchmark values (at $P_{RPP} = 140$ mmHg) reveals that the increased DVR inflow (from 8 to 12 nl/min) elevated DVR flow. This increased fluid delivery to the IM washed out the IM axial solute gradient. As a result, DVR osmolality was reduced by 150 mosmol/kgH$_2$O at the papillary tip and urine osmolality fell from 805 to 645 mosmol/kgH$_2$O.

In the antidiuretic model, the degree of MBF autoregulation exerts significant control over urine flow rate, osmolality, and urea excretion rate, while the NaCl excretion rate is almost completely insensitive to elevated MBF.

*Medullary blood flow autoregulation in diuresis.* Similar to the antidiuretic model, increased $K_{MBF}$ in the diuretic model elevates urine flow rate and urea excretion rate, and decreases urine osmolality (see Fig. 7). The rate of NaCl excretion remained highly insensitive to $K_{MBF}$ but, in contrast to the antidiuretic model, varied inversely to changes in $K_{MBF}$. Comparing the urine at $P_{RPP} = 100$ and 200 mmHg shows that the
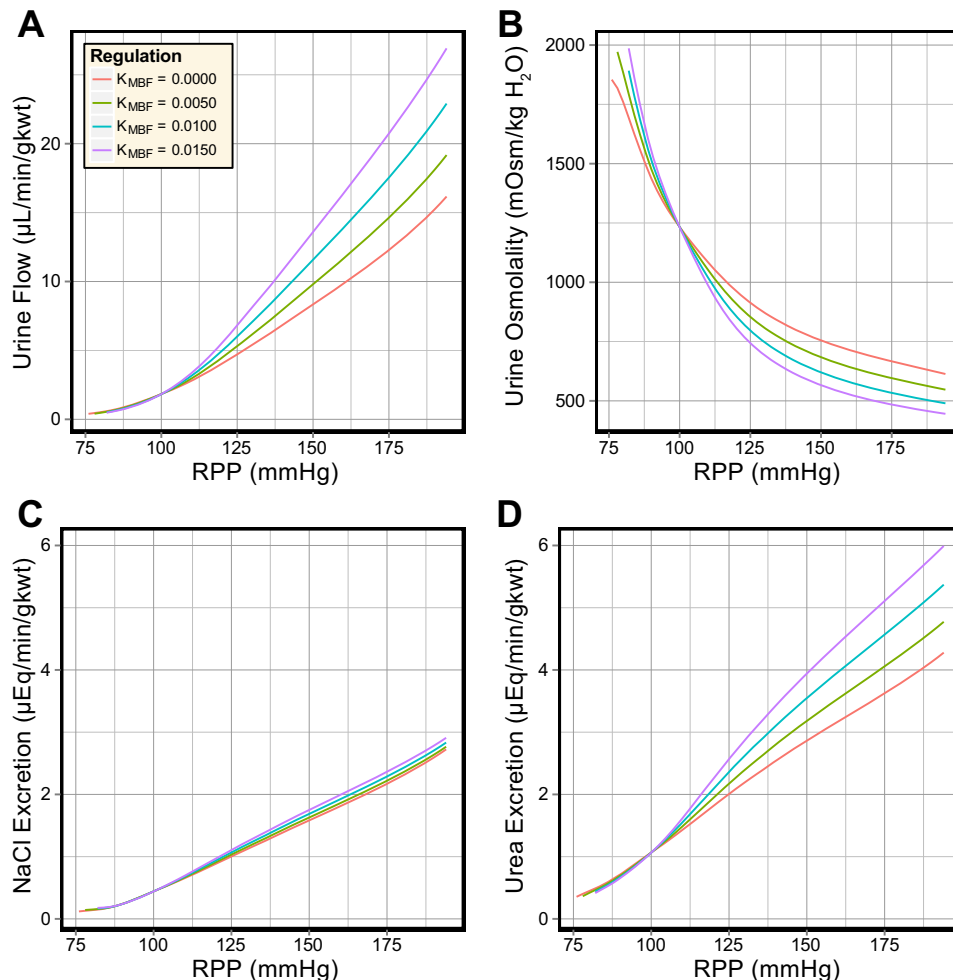


Fig. 6. Effects of different degrees of medullary blood flow (MBF) autoregulation in the antidiuretic model. In response to elevated perfusion pressure: urine flow increases 6- to 12-fold (*A*); urine osmolality decreases by ~60% (*B*); NaCl excretion increases 5- to 6-fold (*C*); and urea excretion increases 4- to 6-fold (*D*).
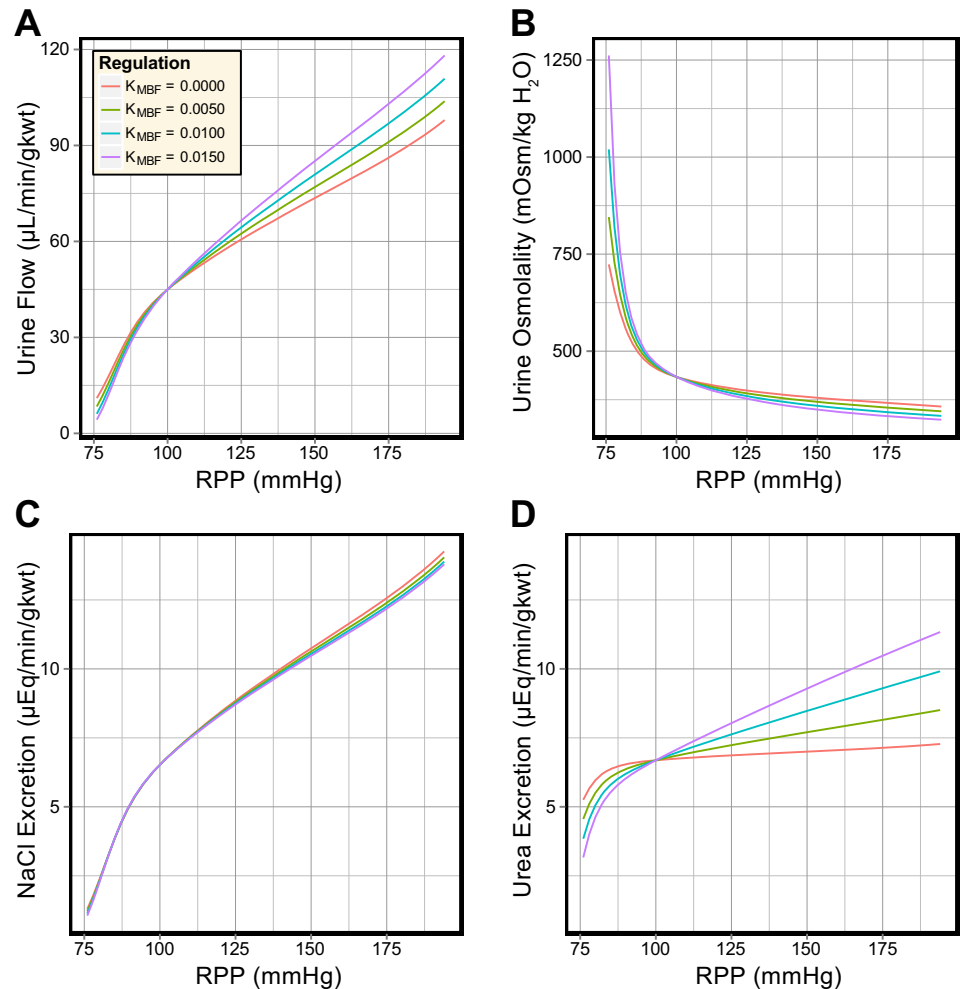
Fig. 7. Effects of different degrees of MBF autoregulation in the diuretic model. In response to elevated perfusion pressure: urine flow increases 2-fold (*A*); urine osmolality decreases by around 25% (*B*); NaCl excretion increases 2-fold (*C*); and urea excretion increases by 10–70% (*D*).

relative increases in excretion rates and the decrease in urine osmolality are significantly smaller in the diuretic model than in the antidiuretic model. For example, NaCl excretion varied by only 3.4% at the maximal perfusion pressure (194 mmHg).

The decrease in NaCl excretion as $K_{MBF}$ increases is due to the large difference in baseline urine flow rate. In the antidiuretic and diuretic models, urine NaCl concentrations are comparable. At $P_{RPP} = 140$ mmHg in the antidiuretic model, increased MBF elevates urine flow by 3.9 $\mu l \cdot min^{-1} \cdot g$ kwt$^{-1}$, a relative change of 58%. In the diuretic model, the same increase in MBF elevates urine flow by 7.5 $\mu l \cdot min^{-1} \cdot g$ kwt$^{-1}$, a relative change of 11%.

In the diuretic model, volume expansion significantly diminishes the sensitivity of the urine flow rate, osmolality, and solute excretion rates to the degree of MBF autoregulation. The additional washout caused by the increased MBF has only a minimal effect on the model urine.

*PCT response in antidiuresis.* In these simulations, DVR inflow was fixed at 8 nl/min and the slope of the PCT response ($K_{PCT}$) was set to 0.010, 0.025, and 0.040. The values represent diminished, normal, and elevated PCT transport inhibition and affect the PST inflow rates at the corticomedullary boundary. Model urine volume and composition are shown in Fig. 8. Model SNGFR was well regulated and did not differ significantly from the simulations where $K_{MBF}$ was varied.

Increasing $K_{PCT}$ from 0.010 to 0.025 greatly increased the sensitivity of the urine flow rate, osmolality, and solute excretion rates to the renal perfusion pressure. Increasing $K_{PCT}$ further to 0.040 had a similar additional effect.

When $P_{RPP}$ was raised from 100 to 194 mmHg, urine flow rate increased 5- to 10-fold, urine osmolality decreased by 41–52%, NaCl excretion increased 4–7-fold, and urea excretion increased by 290–440%. Comparing the antidiuretic model sensitivity to changes in $K_{MBF}$ and $K_{PCT}$, the most significant difference is that the NaCl excretion rate is much more sensitive to $K_{PCT}$ than to $K_{MBF}$.

The increased PST delivery caused by increases in $K_{PCT}$ led to elevated CD volume delivery. At $P_{RPP} = 140$ mmHg, CD fractional volume reabsorption was diminished from 90% ($K_{PCT} = 0.010$) to 84.5% ($K_{PCT} = 0.025$) and 80% ($K_{PCT} = 0.040$). However, net CD volume reabsorption was increased from 6.52 to 7.11 and 7.47 nl·min$^{-1}$·CD$^{-1}$. The difference in urine flow rate for these values of $K_{PCT}$ was 4.9 $\mu l \cdot min^{-1} \cdot g$ kwt$^{-1}$, which was smaller than the difference in OMCD delivery (9.1 $\mu l \cdot min^{-1} \cdot g$ kwt$^{-1}$). The increased CD volume delivery also reduced the solute concentrations along the CD and reduced urine osmolality from 986 to 805 and 718 mosmol/kgH$_2$O. Urine NaCl and urea concentrations varied by 38 and 138 mM as a result of the variations in $K_{PCT}$. In
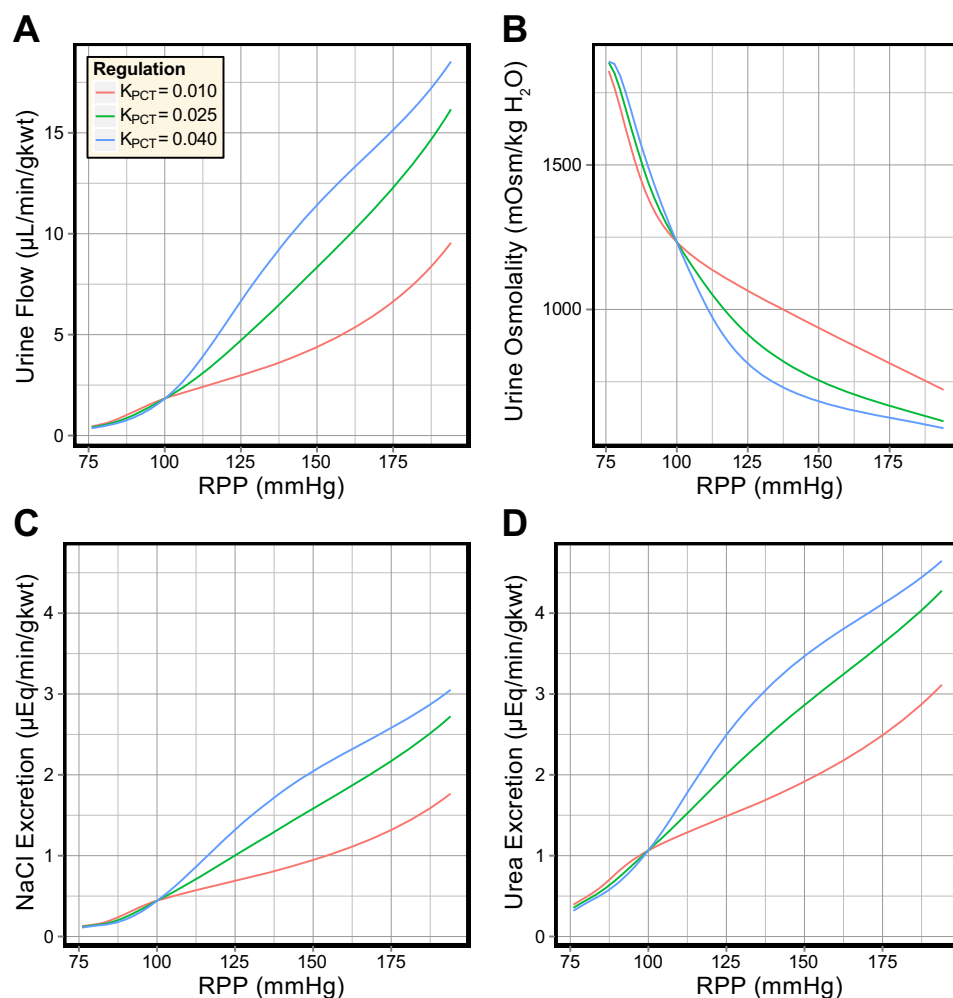
Fig. 8. Effects of different degrees of transport inhibition in the PCT in the antidiuretic model. In response to elevated perfusion pressure: urine flow is significantly regulated by the PCT response (*A*); urine osmolality is significantly regulated by the PCT response (*B*); NaCl excretion is significantly regulated by the PCT response (*C*); and urea excretion is significantly regulated by the PCT response (*D*).

contrast, varying $K_{MBF}$ produced near-identical changes in urine NaCl and urea concentration.

In the antidiuretic model, the slope of the PCT response exerted significant influence on urine flow rate, osmolality, and solute excretion rates. However, elevated MBF produced larger pressure-sensitive variations in urine flow rate, osmolality, and urea excretion rate (compare Fig. 6 to Fig. 8).

*PCT response in diuresis.* Variations in the PCT response in the diuretic model are shown in Fig. 9, for the same range of $K_{PCT}$ values. Urine flow rate and NaCl excretion are significantly elevated ($\approx$10-fold) in the diuretic model, and the urine osmolality is significantly diminished. The most significant difference between the antidiuretic and diuretic model sensitivity to $K_{PCT}$ is urea excretion, which is highly sensitive to $K_{PCT}$ in the antidiuretic model and consistently exceeds the NaCl excretion rate. In the diuretic model, the urea excretion rate exhibits almost complete insensitivity to $K_{PCT}$ and varies by only 4% at $P_{RPP} = 194$ mmHg. Urea excretion is also consistently lower than NaCl excretion in the diuretic model.

We now compare flow rate and solute concentration profiles for the benchmark values of $K_{PCT}$ (0.010, 0.025, and 0.040) at $P_{RPP} = 140$ mmHg. Increased PCT reabsorption inhibition elevated volume delivery to the descending limbs, which was not negated by an increase in volume reabsorption along the descending limbs. OMCD inflow rate was elevated in propor-

tion to $K_{PCT}$, from 17.3 ($K_{PCT} = 0.010$) to 19.6 ($K_{PCT} = 0.025$) and 21.4 nl·min$^{-1}$·CD$^{-1}$ ($K_{PCT} = 0.040$). Fractional CD volume reabsorption decreased when $K_{PCT}$ was increased (from 38 to 33 and 30%) but absolute CD volume reabsorption remained fixed at 6.55 nl·min$^{-1}$·CD$^{-1}$. Urine NaCl concentration varied by <1 mM in response to $K_{PCT}$, while urine urea concentration decreased by 30 mM. This decrease in urine urea concentration was almost exactly countered by the increase in urine flow rate, resulting in near-constant urea excretion.

In the diuretic model, variations in the slope of the PCT response produced smaller relative changes in urine flow rate, osmolality, and solute excretion rates than those in the antidiuretic model. Urea excretion was near constant, a result of the limited urea recycling in the IM in diuresis. The absolute increases in urine flow rate and NaCl excretion rate, in response to elevated perfusion pressure, were significantly larger in the diuretic model than in the antidiuretic model. The relative increase in these excretion rates were, however, smaller than in the antidiuretic model. This is consistent with the differences between the pressure natriuresis observed in the antidiuretic and the diuretic rat (33, 34, 82).

*Combined regulation in antidiuresis.* The sensitivity of the model to simultaneous variations in both MBF and transport inhibition in the PCT was assessed (see Fig. 10). In the antidiuretic rat, MBF is as strongly autoregulated as the cortical
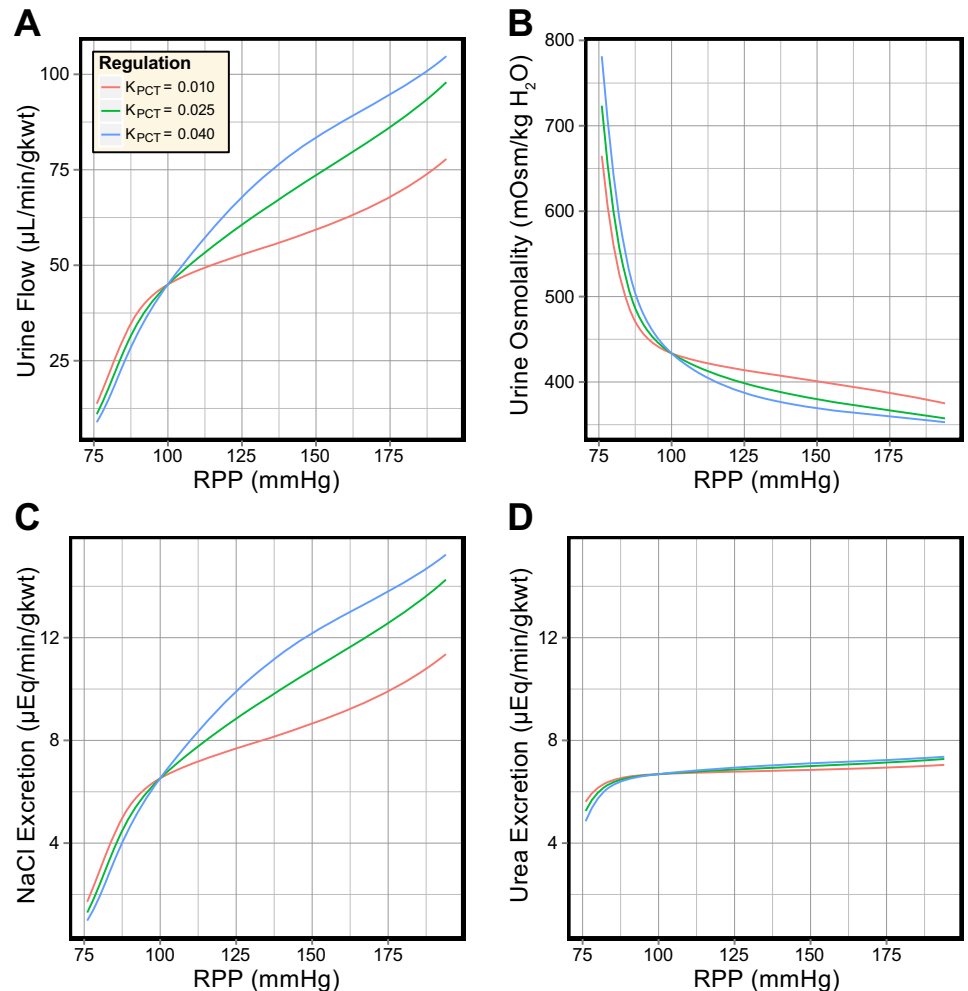
Fig. 9. Effects of different degrees of transport inhibition in the PCT in the diuretic model. In response to elevated perfusion pressure: urine flow is significantly regulated by the PCT response (*A*); urine osmolality is somewhat regulated by the PCT response (*B*); NaCl excretion is significantly regulated by the PCT response (*C*); and urea excretion is insensitive to the PCT response (*D*).

blood flow (33, 65). This suggests that the curves for $K_{MBF} = 0$ should be representative for the antidiuretic model. In the model, decreased MBF autoregulation elevated urine flow and urea excretion and diminished the urine osmolality, while having little effect on NaCl excretion. On the other hand, the PCT response played a dominant role in driving pressure natriuresis in the model, regardless of MBF autoregulation.

The increase in $K_{MBF}$ reduced urea secretion into the long descending limbs by 2–3%, while increasing $K_{PCT}$ reduced urea secretion by 13–20%. This suggests that MBF autoregulation has a lesser impact than the PCT response on urea recycling in the IM. Net volume reabsorption along the CD was significantly enhanced when MBF was strongly autoregulated, while the PCT response played a greater role in determining the OMCD inflow rate.

*Combined regulation in diuresis.* In the diuretic model, PCT reabsorption inhibition and weak MBF autoregulation (as observed in volume-expanded rats) have synergistic effects. Urine flow rate was elevated and urine osmolality was decreased (see Fig. 11). Urea excretion exhibits no sensitivity to $K_{PCT}$ but was sensitive to MBF. Similar to the antidiuretic model, NaCl excretion was highly sensitive to the PCT response and showed minimal sensitivity to MBF autoregulation. In contrast to the antidiuretic model, decreased MBF autoregulation slightly diminished NaCl excretion (as remarked upon earlier).

The DVR flow rate and osmolality, and the NaCl and urea concentrations in the loops of Henle, showed much less sensitivity to both the PCT response and MBF autoregulation than observed in the antidiuretic model. The interstitial washout that accompanies volume expansion limited the effects of these mechanisms. Decreased CD water permeability meant that $K_{MBF}$ and $K_{PCT}$ could produce only minimal differences in volume reabsorption along the CD, contrary to the antidiuretic model. Decreased IMCD urea permeability in the diuretic model permitted only minimal urea recycling, regardless of the IMCD urea flow rate. Urea excretion was two to three times higher in the diuretic model than in the antidiuretic model and urine osmolality did not exceed 430 mosmol/kgH$_2$O when $P_{RPP} \geq 100$ mmHg.

*Acute in vivo pressure natriuresis.* The rates of water and NaCl excretion in the antidiuretic and diuretic models were then compared with experimental measurements of acute renal function in the rat (see Fig. 12, *A* and *B*). The majority of experimental studies observed strong autoregulation of RBF and GFR over wide ranges of perfusion pressure (from 90 to 200 mmHg) (33, 34, 38, 41, 56, 58, 60, 62, 74, 83), while other studies measured significant increases in RBF and/or GFR (57, 64, 66, 101, 103). There does not appear to be a factor in the chosen cohorts or experimental methods that determines whether RBF and GFR are strongly or weakly regulated. Both RBF and whole kidney GFR were also observed to decrease
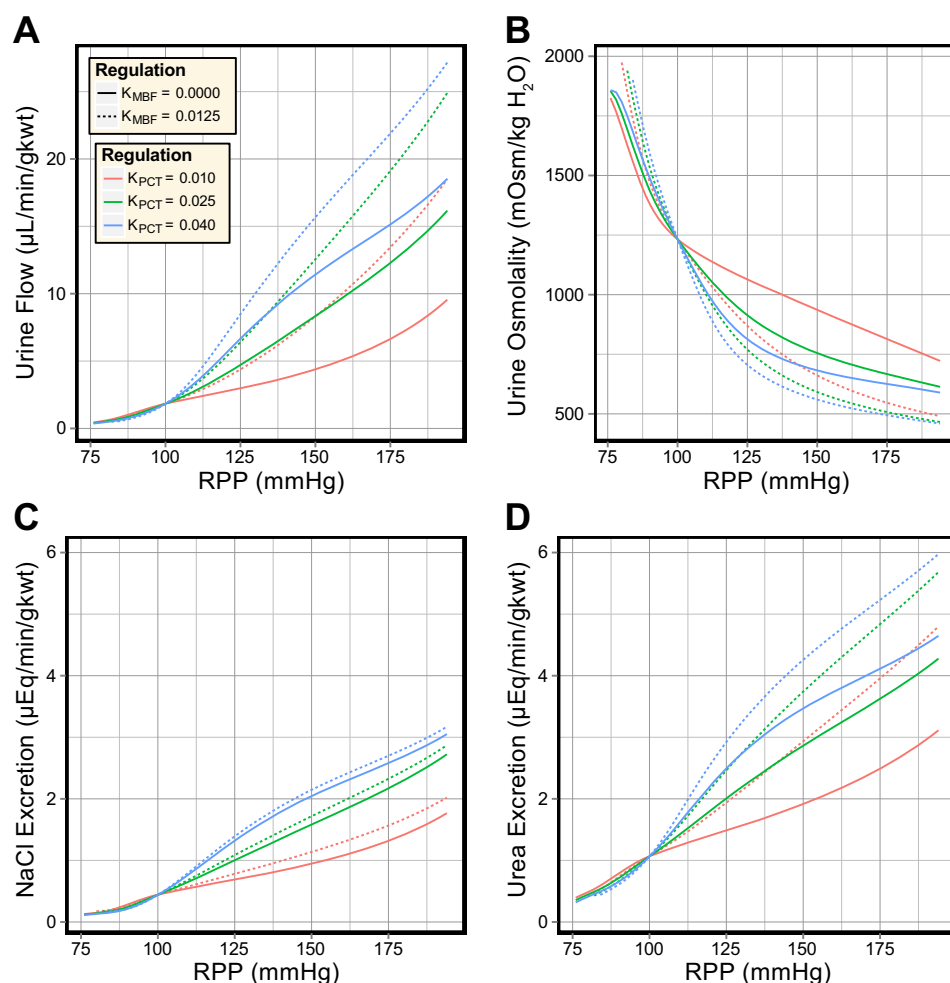
Fig. 10. Effects of varying both the degree of MBF autoregulation and the degree of transport inhibition in the PCT in the antidiuretic model. In response to elevated perfusion pressure: urine flow is more sensitive to MBF autoregulation than to transport inhibition in the PCT (*A*); urine osmolality is more sensitive to MBF autoregulation than to transport inhibition in the PCT (*B*); NaCl excretion is more sensitive to transport inhibition in the PCT than to MBF autoregulation (*C*); urea excretion is more sensitive to MBF autoregulation than to transport inhibition in the PCT (*D*).

below control levels at low perfusion pressures ($P_{RPP} \leq 90$ mmHg) in the antidiuretic kidney.

The rates of water and NaCl excretion in the antidiuretic model compared well to the minimal rates observed across the range of surveyed studies. In contrast, the agreement between the diuretic model and experimental data was less ideal. This is likely attributable to the PCT response and/or the CD epithelial parameters. Thus, in subsequent simulations, we attempted to fit the diuretic model excretion rates to whole kidney excretion data. This was achieved by adjusting the PCT response and by altering the model CD transport parameters.

From the experimental studies shown in Fig. 12, *A* and *B*, a single study was chosen and used to fit the model excretion curves. Guarasci and Kline (38) investigated acute pressure natriuresis in the rat following both acute and chronic inhibition of nitric oxide synthase (NOS), which inhibits the regulatory effects of nitric oxide (NO) in the renal medulla. This study was selected on the basis that the animals exhibited strong pressure-natriuresis responses and that the absence of NO from the model formulation matches the experimental conditions. PCT responses were fitted to the two groups of rats: "Control" and "L-NAME." For each group, model excretion curves were fitted under two assumptions: that there is active NaCl transport along the model CD (as in the antidiuretic model) and that this active transport is inhibited in diuresis (as suggested by some studies; Refs. 50, 52, 70, 94, 96, 98).

In each case, the parameters in *Eq. 24* that govern PCT fractional reabsorption ($K_0$, $K_1$, and $K_{Op}$) were adjusted so that the model NaCl excretion rate resembled the measurements of Guarasci and Kline (38). The resulting PCT response curves are shown in Fig. 13. The agreement between the model urine flow and experimental data was also much improved (compare Fig. 12, *A* and *C*).

The diuretic model excretion curves provided a good match to the experimental excretion rates when the fitted PCT responses were used. Whether these PCT responses are consistent with experimental observations of reabsorption in the PCT under saline diuresis is another matter. We address this question in the DISCUSSION.

## DISCUSSION

The model only incorporates a few regulatory mechanisms: the myogenic response of the afferent arteriole, TGF, the direct effects of MBF on medullary solute concentrations, and inhibition of water and NaCl transport in the PCT. The model does not account for the actions of the renin-angiotensin system (RAS), NO, or endothelin, all of which are known to play significant roles in the regulation of renal NaCl excretion. Furthermore, MBF is understood to initiate signaling cascades (via RIHP) that affect sodium reabsorption in the PCT (67). Thus the regulatory mechanisms in the model are both highly
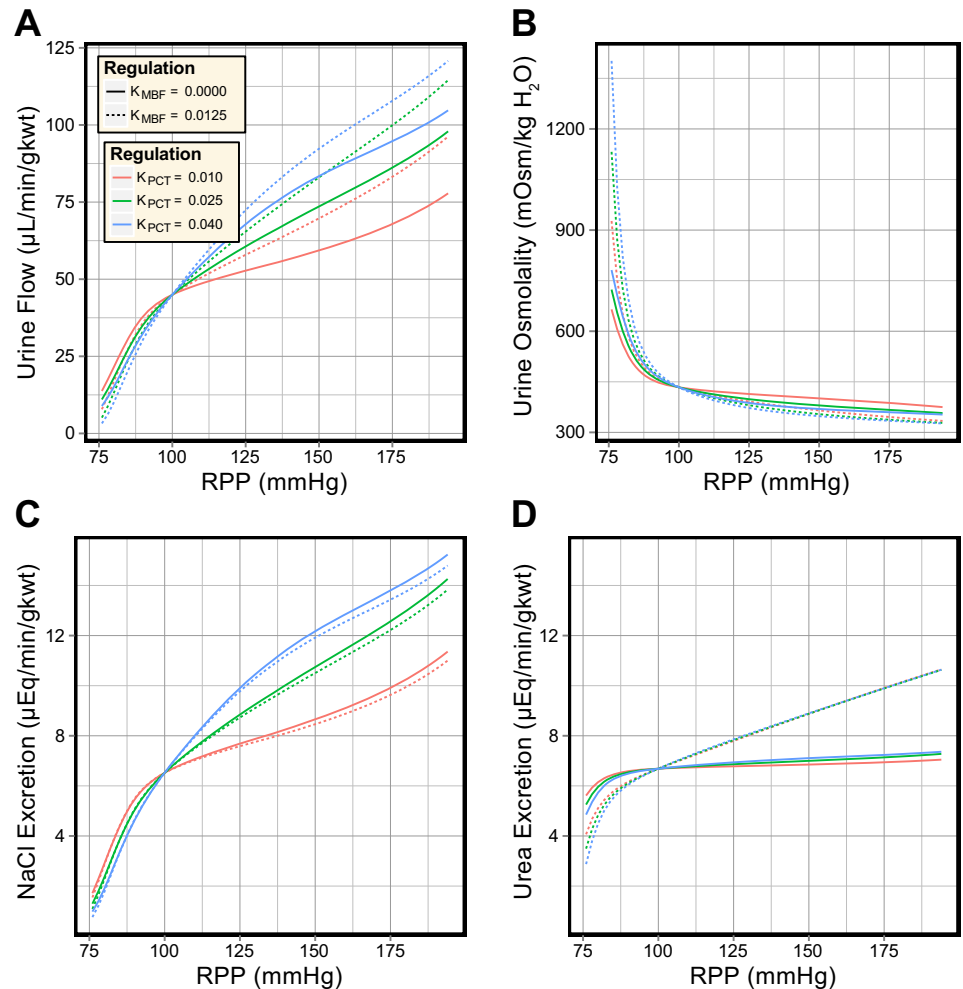
Fig. 11. Effects of varying both the degree of MBF autoregulation and the degree of transport inhibition in the PCT in the diuretic model. In response to elevated perfusion pressure: urine flow is more sensitive to MBF autoregulation than to transport inhibition in the PCT (*A*); urine osmolality is slightly more sensitive to MBF autoregulation than to transport inhibition in the PCT (*B*); NaCl excretion is more sensitive to transport inhibition in the PCT than to MBF autoregulation (*C*); urea excretion is more sensitive to MBF autoregulation than to transport inhibition in the PCT (*D*).

simplified and incomplete. This is due, in part, to a shortage of relevant (quantitative) experimental data.

However, these limitations do not necessarily invalidate interpretation of the results presented in this article. In experimental studies of acute pressure natriuresis (such as those shown in Fig. 12), the experimental protocols include measures to keep paracrine levels fixed. This is typically achieved by steady infusion of a "cocktail" of hormones and various inhibitors/antagonists. Short stabilization and collection periods (e.g., 5–20 min) are also used to ensure there is insufficient time for other, slower, regulatory mechanisms to respond.

In short, in the experimental studies of acute pressure natriuresis against which we have compared our model, the very paracrine factors we have been unable to incorporate into our model have been either inhibited or maintained at fixed physiological levels. However, conclusions drawn from the model results may not apply to pressure natriuresis in organisms whose paracrine levels are not tightly controlled. Keeping these limitations in mind, we now compare the model MBF and PCT responses to in vivo data to evaluate the degree to which the model dynamics are consistent with experimental observations.

*Medullary blood flow autoregulation.* Medullary blood flow is known to be strongly autoregulated in antidiuretic rats (24, 33, 65) and weakly regulated in diuretic rats (33, 66, 82). The

benchmark values for $K_{MBF}$ used in this study (0 and 0.0125) correspond to the regulatory responses observed in hydropenic and volume-expanded rats (65). Since the experimental techniques used to measure variations in MBF are not capable of measuring absolute flow rates, the only quantitative data against which the model DVR flow rates can be compared are micropuncture measurements at the papillary tip.

Blood flow rate in individual DVR vessels at the papillary tip has been measured in several studies and has consistently been measured at 8–11 nl/min in volume-expanded rats (40, 105, 106). In the model base cases, the papillary DVR plasma flow rate is 5.0 nl/min in the antidiuretic model and 7.3 nl/min in the diuretic model (for an individual DVR vessel). Experimental measurements of papillary DVR hematocrit range from 9 to 21% (40). This would imply blood flow rates of 5.5–6.3 and 8.0–9.2 nl/min in the papillary DVR of the antidiuretic and diuretic models, respectively. The papillary DVR flow rate in the diuretic model is consistent with the experimental observations, while the papillary DVR flow rate in the antidiuretic model (5.5–6.3 nl/min) is lower than that observed by Holliger et al. (40) in young antidiuretic rats (8.83 nl/min).

In the diuretic model, decreased autoregulation of MBF (i.e., interstitial washout) did not stimulate an increase in NaCl excretion. This is consistent with evidence that increased washout is not a dominant factor in pressure natriuresis (21, 28,
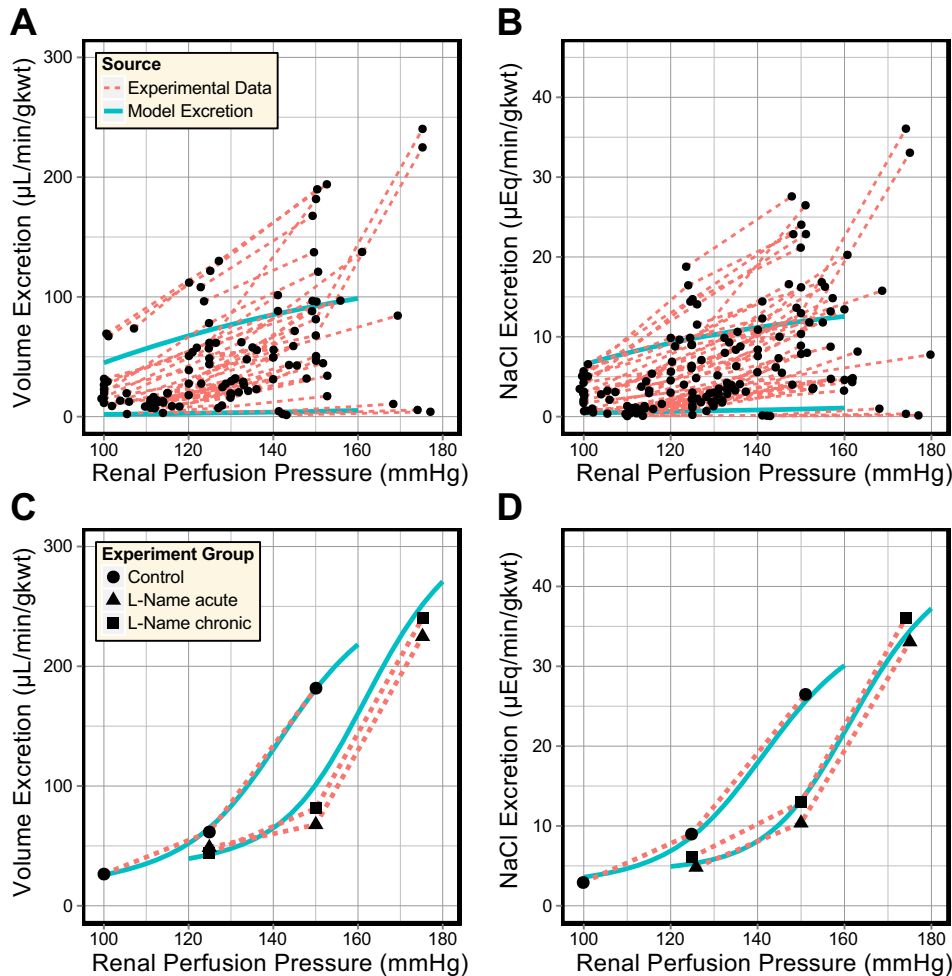
Fig. 12. Regulation of water (*A*) and salt (*B*) excretion in the antidiuretic model ($K_{MBF} = 0$, $K_{PCT} = 0.010$, lower curve) and diuretic model ($K_{MBF} = 0.0125$, $K_{PCT} = 0.040$, upper curve), compared with acute renal function data obtained from studies in the rat (33, 34, 38, 41, 56–58, 60, 62, 64, 66, 74, 83, 101). PCT responses were then fitted (*C* and *D*) to a single study of acute pressure-natriuresis in which nitric oxide synthase was inhibited (38).

85). Likewise, decreased autoregulation of MBF in the antidiuretic model did not increase NaCl excretion, since the increased urine flow rate was countered by an equivalent decrease in urine NaCl concentration (Fig. 6). Thus, while MBF plays a significant role in maintaining the hydration status, the model predictions suggest that its direct effects on the interstitial composition have negligible consequences for pressure natriuresis. It remains unclear whether MBF can trigger phenomena such as reduced PCT reabsorption or if the observed correlation between MBF autoregulation and NaCl excretion is due to a common (unidentified) mechanism, such as elevated RIHP (34, 37, 44, 48). The degree of MBF autoregulation is strongly influenced by circulating levels of vasopressin (23, 33), which indicates that vasopressin might play a role in modulating pressure natriuresis. The model results are consistent with the hydration-dependent magnitude of the pressure-natriuresis response and experimental evidence of the effects of interstitial washout. They cannot provide insight into in vivo signaling and the downstream effects of MBF autoregulation.

*NaCl reabsorption in the PCT.* Some studies have suggested that increased NaCl excretion after volume expansion requires alterations in NaCl reabsorption beyond the PCT (50, 52, 70, 94, 96, 98). Sonnenberg (96) observed that "only in the low-salt rats can the natriuresis be explained by inhibition of Na transport in the CD; excretion of NaCl in expanded DOCA rats is uniformly greater than end-distal delivery, indicating net entry of the ion into the terminal nephron segment."

By contrast, fractional NaCl reabsorption along the CD was consistently 10–20% in the diuretic model. Net NaCl secretion into the CD was not observed. It is therefore important to determine whether the fitted PCT responses (shown in Fig. 13) are consistent with experimental measurements of PCT reabsorption under saline diuresis. Inconsistencies between the model PCT response and experimental data would suggest that some of the diuretic parameter values (Table 2) are inappropriate. Acute volume expansion has been observed to reduce PCT fractional reabsorption from 61 to 42% (perfusion/arterial pressure not reported) (53) and from 62% ($P_{RPP} = 114$ mmHg) to 33% ($P_{RPP} = 110$ mmHg) (11). Under saline diuresis, increased perfusion pressure has been observed to reduce PCT fractional reabsorption even further, from 65% ($P_{RPP} \approx 80$ mmHg) to as low as 25% ($P_{RPP} \approx 135$ mmHg) (6). An increase of 50% in PCT delivery to the descending limb [as observed by Brenner et al. (11), mentioned above] is consistent with in vivo observations of end proximal tubule fluid velocity and flow rate in response to acute arterial hypertension (105→155 mmHg) in the rat (19). Urine flow rate was also increased ~2.5-fold in response to the acute hypertension. A smaller degree of hypertension (104→129 mmHg) was observed to increase urine flow by 45 and late proximal flow rate by 30% (18). Clearly, there
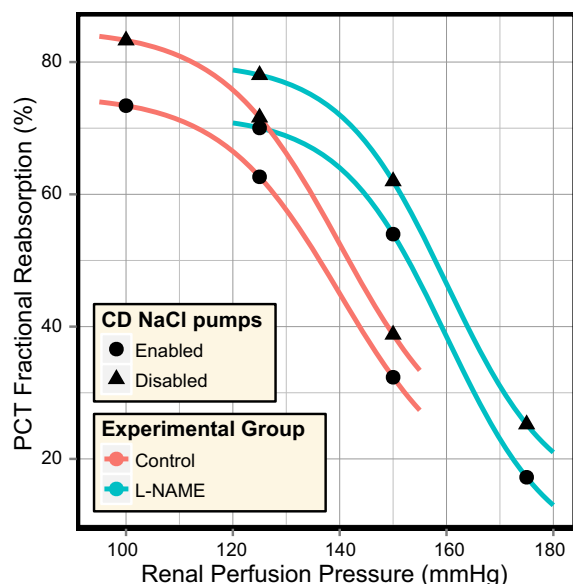
Fig. 13. A comparison of the PCT responses fitted to the excretion rates measured by Guarasci and Kline (38), when active transport of NaCl in the model CD is enabled and when it is disabled.

is significant variation between the baseline reabsorption rates and between the magnitude of the changes in reabsorption in response to volume expansion and acute hypertension.

Guarasci and Kline (38) observed an approximately five- to sixfold increase in urine flow rate and a seven to eightfold increase in NaCl excretion rate in response to an acute perfusion pressure elevation of 50 mmHg (Fig. 4). The PCT responses fitted to the "Control" case, with and without CD NaCl active transport, are consistent the above data. Volume expansion, without elevation in perfusion pressure, was observed in vivo to decrease PCT fractional reabsorption to 30–40%. When combined with an acute elevation of perfusion pressure to 135 mmHg, in vivo PCT fractional reabsorption decreased to 25%. PCT fractional reabsorption for both fits is significantly higher at $P_{RPP} = 100$ mmHg than observed in volume-expanded animals. Instead, it is more consistent with levels observed in vivo before volume expansion. The decrease in fractional reabsorption from $P_{RPP} = 125$ mmHg to $P_{RPP} = 150$ mmHg is larger than observed in vivo, where late proximal flow rate increased by 30% and urine flow rate increased by 45% (18), but the pressure natriuresis observed by Guarasci and Kline (38) was also much larger than that observed by Chou and Marsh (18).

The PCT responses fitted to the "L-NAME" case predicted end-proximal flows and urine flows that were consistent with in vivo measurements in response to an acute elevation from $P_{RPP} = 125$ mmHg to $P_{RPP} = 150$ mmHg (18). Since PCT fractional reabsorption has been observed as low as 25% at $P_{RPP} = 135$ mmHg (6), it seems plausible that it should decrease further when the perfusion pressure is elevated to 175 mmHg. This remains plausible, even when accounting for the shift of the pressure-natriuresis response induced by the administration of nitro-L-arginine methyl ester (L-NAME), as observed by Guarasci and Kline.

Studies have suggested that CD NaCl reabsorption is inhibited under volume expansion (50, 52, 70, 94), and NaCl

secretion into the CD has even been observed (96–98). This suggests that the diuretic model is, perhaps, more realistic when active NaCl transport along the CD is inhibited. However, while PCT fractional reabsorption has been measured to be as high as 75% in antidiuretic animals (35), volume expansion is known to significantly reduce PCT reabsorption. Thus PCT fractional reabsorption for the fitted responses is higher than expected at the lowest pressures ($P_{RPP} = 100$ mmHg for "Control" and $P_{RPP} = 125$ mmHg for "L-NAME"), while being consistent with in vivo data at higher pressures. This suggests that the diuretic model (Table 2) produces a diuresis that is too strong at these low pressures and that PCT reabsorption must be overly elevated to counter this. This could be avoided by scaling the diuresis in proportion to the model perfusion pressure.

Given that the slope of the whole kidney pressure natriuresis response is commonly observed to be around four to six times steeper in diuretic animals than in antidiuretic animals (34, 60, 64, 74, 78, 80, 82, 103), it is reasonable to suggest that the model PCT response in the diuretic model should also be four to six times steeper than in the antidiuretic model. The slope of the fitted PCT responses in the diuretic model varied from 0.09 to 0.10, which is four times larger than the slope considered reasonable for the antidiuretic model (0.025).

Plasma ADH is known to increase the water permeability of the late distal tubule and CD (12, 27, 31, 42), to increase the urea permeability of the IMCD (42, 88, 90), and to stimulate active NaCl transport along the CD (39, 42, 61, 77). The epithelial changes introduced in the diuretic model are consistent with the known effects of the decrease in circulating ADH that is caused by volume expansion. Therefore, the model results suggest that the known actions of decreased ADH levels and increased inhibition of reabsorption in the PCT are sufficient to drive pressure natriuresis to levels consistent with those observed in experimental studies. The mechanisms by which PCT reabsorption is inhibited under volume expansion remain insufficiently quantified and cannot be investigated with this model.

*Regulation of urea excretion.* In all mammals investigated, urea excretion has been observed to vary with the protein content of the diet (91), which is beyond the scope of this model. Urea excretion is also regulated by ADH (86, 87), which stimulates urea reabsorption in the terminal IMCD, and so we should expect the model urea excretion rate to be elevated in the diuretic kidney. Model excretion rates were 1–6 μeq·min$^{-1}$·g kwt$^{-1}$ in the antidiuretic model and 7–11 μeq·min$^{-1}$·g kwt$^{-1}$ in the diuretic model (compare Figs. 10 and 11). Model urine urea concentrations were 220–580 mM in the antidiuretic kidney and 70–150 mM in the diuretic kidney. In both cases, the concentration was maximal at low perfusion pressures and decreased in response to elevations in perfusion pressure.

Urea excretion has been measured in various studies in the rat. In male Sprague- Dawley rats an acute elevation of perfusion pressure by 37 mmHg doubled the urea excretion rate from 3.7 to 7.5 μeq·min$^{-1}$·g kwt$^{-1}$ (81). In response to acute elevations of around 60 mmHg in male Wistar-Kyoto rats, urea excretion increased from 2.7 to 5.5 μeq·min$^{-1}$·g kwt$^{-1}$ (80). In male spontaneously hypertensive rats, the same elevation increased urea excretion from 4.1 to 5.0 μeq·min$^{-1}$·g kwt$^{-1}$ (80). Water diuresis in male Wistar rats produced a rapid

increase in urea excretion that returned to nondiuretic levels after 6–8 h (5). Osmotic diuresis also produced a rapid increase in urea excretion before decreasing to levels around 50% higher than in the nondiuretic rat (5). Saline diuresis in male Wistar rats elevated the urea excretion rate from 2.7 to 7.5 $\mu$eq·min$^{-1}$·g kwt$^{-1}$ in dehydrated rats, from 4.0 to 6.7 $\mu$eq·min$^{-1}$·g kwt$^{-1}$ in "normal" rats, and from 2.7 to 5.4 in hydrated rats (4). In response to ADH infusion in male Wistar rats, it was observed that "plasma urea concentrations were lowest in the diuretic groups, where the high urine flows were associated with the highest urinary urea outputs and urea clearances" (3).

In the antidiuretic model, urea excretion rate was increased from 1.1 to 3.1 $\mu$eq·min$^{-1}$·g kwt$^{-1}$ in response to acute elevations of 40 mmHg ($K_{MBF} = 0$, $K_{PCT} = 0.040$) and 60 mmHg ($K_{MBF} = 0$, $K_{PCT} = 0.025$), similar to the observations in Sprague-Dawley and Wistar-Kyoto rats. Acute elevations in the diuretic model produced smaller fractional increases in urea excretion rate, from 6.6 to 8.4 $\mu$eq·min$^{-1}$·g kwt$^{-1}$ (40 mmHg) and 9.2 $\mu$eq·min$^{-1}$·g kwt$^{-1}$ (60 mmHg), comparable to the observations in spontaneously hypertensive rats. At $P_{RPP} = 100$ mmHg the urea excretion rates in the antidiuretic and diuretic models were 1.1 and 6.6 $\mu$eq·min$^{-1}$·g kwt$^{-1}$, respectively, which is comparable to the effects of saline diuresis in dehydrated male Wistar rats (from 2.7 to 7.5 $\mu$eq·min$^{-1}$·g kwt$^{-1}$). In all model simulations it was observed that increased urine flow was accompanied by decreased urine urea concentration and increased urea excretion, consistent with the behavior observed in Wistar rats undergoing ADH infusion. This suggests that the model urine concentrating mechanism degrades in a realistic manner.

*Anatomical considerations.* Juxtamedullary afferent arterioles exhibit efficient blood flow autoregulation in the rat (14, 100), even in response to volume expansion (29, 43, 79, 95). If the DVR inflow rate is determined solely by the efferent flow rate of the juxtamedullary nephron population, this implies that MBF must be well-regulated in diuresis, which appears to contradict experimental measurements of MBF in diuretic rats (32, 33, 65). Roman et al. (82) suggested that the vascular resistance of the DVR might decrease when RPP is elevated. In the model simulations presented here, we have ignored this issue and varied the DVR inflow independently of the juxtamedullary SNGFR, but we can speculate as to how these two quantities may vary independently of each other in vivo.

Preglomerular shunts have been observed in the rat kidney (15), although the role of these vessels remains uncertain (72). If we assume that such shunts exist in a small fraction of the juxtamedullary nephron population and that their endothelium is similar to that of the initial DVR (46), then it seems plausible that such vessels could be closed and admit no flow of plasma or renal blood cells when the circulating levels of ADH are relatively high and that such vessels could be open and admit the flow of plasma and renal blood cells when the circulating levels of ADH are relatively low (69, 71). This would explain how juxtamedullary SNGFR and DVR can be regulated independently and why the rate of MBF is dependent upon the hydration status of the animal.

*Conclusions.* The model has been used to predict pressure-sensitive changes in NaCl excretion in response to variations in MBF autoregulation and inhibition of PCT reabsorption. Changes in epithelial permeability, representing physiological

effects of volume expansion, were shown to increase model NaCl and water excretion rates, but these increases are insensitive to the perfusion pressure.

The results also suggest that the direct effects of MBF on the interstitial composition cannot stimulate pressure natriuresis. In both the antidiuretic and diuretic models, MBF autoregulation exerted a stronger effect on urine osmolality and flow rate than did the PCT response. This suggests that efficient MBF autoregulation, as observed in the antidiuretic rat, is important for maintaining the whole body hydration status.

Model PCT responses were fitted to produce water and solute excretion rates that matched experimental measurements of pressure natriuresis in the diuretic rat. These responses were consistent with experimental observations of PCT reabsorption inhibition, suggesting that inhibition of PCT reabsorption is sufficient to drive pressure natriuresis to levels observed in vivo. The signaling mechanisms that mediate this inhibition are presumably key factors responsible for stimulating pressure natriuresis.

## DISCLOSURES

No conflicts of interest, financial or otherwise, are declared by the author(s).

## AUTHOR CONTRIBUTIONS

Author contributions: R.M. and A.T.L. conception and design of research; R.M. performed experiments; R.M. and A.T.L. analyzed data; R.M. and A.T.L. interpreted results of experiments; R.M. prepared figures; R.M. drafted manuscript; R.M. and A.T.L. edited and revised manuscript; R.M. and A.T.L. approved final version of manuscript.

## REFERENCES

1. **Aperia AC, Broberger CG, Söderlund S.** Relationship between renal artery perfusion pressure and tubular sodium reabsorption. *Am J Physiol* 220: 1205–1212, 1971.
2. **Armsen T, Reinhardt HW.** Transtubular movement of urea at different degrees of water diuresis. *Pflügers Arch* 326: 270–280, 1971.
3. **Atherton JC, Evans JA, Green R, Thomas S.** Influence of variations in hydration and in solute excretion of the effects of lysine-vasopressin infusion on urinary and renal tissue composition in the conscious rat. *J Physiol* 213: 311–327, 1971.
4. **Atherton JC, Green R, Thomas S.** Effects of 0–9% saline infusion on urinary and renal tissue composition in the hydropaenic, normal and hydrated conscious rat. *J Physiol* 210: 45–71, 1970.
5. **Atherton JC, Hai MA, Thomas S.** Effects of water diuresis and osmotic (mannitol) diuresis on urinary solute excretion by the conscious rat. *J Physiol* 197: 395–410, 1968.
6. **Bank N, Koch KM, Aynedjian HS, Aras M.** Effect of changes in renal perfusion pressure on the suppression of proximal tubular sodium reabsorption due to saline loading. *J Clin Invest* 48: 271–283, 1969.
7. **Bengele HH, Lechene C, Alexander EA.** Sodium and chloride transport along the inner medullary collecting duct: effect of saline expansion. *Am J Physiol Renal Fluid Electrolyte Physiol* 238: F504–F508, 1980.
8. **Bertram JF, Soosaipillai MC, Ricardo SD, Ryan GB.** Total numbers of glomeruli and individual glomerular cell types in the normal rat kidney. *Cell Tissue Res* 270: 37–45, 1992.
9. **Bie P.** Blood volume, blood pressure and total body sodium: internal signalling and output control. *Acta Physiol (Oxf)* 195: 187–196, 2009.
10. **Bie P, Damkjær M.** Renin secretion and total body sodium: pathways of integrative control. *Clin Exp Pharmacol Physiol* 37: e34–e42, 2010.

11. **Brenner BM, Troy JL, Daugharty TM, Ueki IF, Nicholas DP, Wong CF.** On the mechanism of inhibition in fluid reabsorption by the renal proximal tubule of the volume-expanded rat. *J Clin Invest* 50: 1596–1602, 1971.

12. **Breyer MD, Ando Y.** Hormonal signaling and regulation of salt and water transport in the collecting duct. *Annu Rev Physiol* 56: 711–739, 1994.

13. **Carlson BE, Arciero JC, Secomb TW.** Theoretical model of blood flow autoregulation: roles of myogenic, shear-dependent, and metabolic responses. *Am J Physiol Heart Circ Physiol* 295: H1572–H1579, 2008.

14. **Carmines PK, Inscho EW, Gensure RC.** Arterial pressure effects on preglomerular microvasculature of juxtamedullary nephrons. *Am J Physiol Renal Fluid Electrolyte Physiol* 258: F94–F102, 1990.

15. **Casellas D, Mimran A.** Shunting in renal microvasculature of the rat: a scanning electron microscopic study of corrosion casts. *Anat Rec* 201: 237–248, 1981.

16. **Cevese A, Guyton AC.** Isohemic blood volume expansion in normal and areflexive dogs. *Am J Physiol* 231: 104–111, 1976.

17. **Chen J, Sgouralis I, Moore LC, Layton HE, Layton AT.** A mathematical model of the myogenic response to systolic pressure in the afferent arteriole. *Am J Physiol Renal Physiol* 300: F669–F681, 2011.

18. **Chou CL, Marsh DJ.** Role of proximal convoluted tubule in pressure diuresis in the rat. *Am J Physiol Renal Fluid Electrolyte Physiol* 251: F283–F289, 1986.

19. **Chou CL, Marsh DJ.** Time course of proximal tubule response to acute arterial hypertension in the rat. *Am J Physiol Renal Fluid Electrolyte Physiol* 254: F601–F607, 1988.

20. **Colding-Jørgensen M, Steven K.** A model of the mechanics of smooth muscle reservoirs applied to the intestinal bladder. *Neurourol Urodyn* 12: 59–79, 1993.

21. **Cowley AW Jr.** Long-term control of arterial blood pressure. *Physiol Rev* 72: 231–300, 1992.

22. **Cowley AW Jr.** Role of the renal medulla in volume and arterial pressure regulation. *Am J Physiol Regul Integr Comp Physiol* 273: R1–R15, 1997.

23. **Cowley AW Jr.** Control of the renal medullary circulation by vasopressin *v*1 and *v*2 receptors in the rat. *Exp Physiol* 85: 223s–231s, 2000.

24. **Cupples WA, Marsh DJ.** Autoregulation of blood flow in renal medulla of the rat: no role for angiotensin II. *Can J Physiol Pharmacol* 66: 833–836, 1988.

25. **Damkjær M, Isaksson GL, Stubbe J, Jensen BL, Assersen K, Bie P.** Renal renin secretion as regulator of body fluid homeostasis. *Pflügers Arch* 465: 153–165, 2013.

26. **Davis MJ, Sikes PJ.** Myogenic responses of isolated arterioles: test for a rate-sensitive mechanism. *Am J Physiol Heart Circ Physiol* 259: H1890–H1900, 1990.

27. **Elalouf JM, Roinel N, de Rouffignac C.** Effects of antidiuretic hormone on electrolyte reabsorption and secretion in distal tubules of rat kidney. *Pflügers Arch* 401: 167–173, 1984.

28. **Evans RG, Majid DS, Eppel GA.** Mechanisms mediating pressure natriuresis: what we know and what we need to find out. *Clin Exp Pharmacol Physiol* 32: 400–409, 2005.

29. **Farman N, Bonvalet JP.** Abnormal relationship between sodium excretion and hypertension in spontaneously hypertensive rats. *Pflügers Arch* 354: 39–53, 1975.

30. **Feldberg R, Colding-Jørgensen M, Holstein-Rathlou NH.** Analysis of interaction between TGF and the myogenic response in renal blood flow autoregulation. *Am J Physiol Renal Fluid Electrolyte Physiol* 269: F581–F593, 1995.

31. **Field MJ, Stanton BA, Giebisch GH.** Influence of ADH on renal potassium handling: a micropuncture and microperfusion study. *Kidney Int* 25: 502–511, 1984.

32. **Franchini KG, Cowley AW Jr.** Sensitivity of the renal medullary circulation to plasma vasopressin. *Am J Physiol Regul Integr Comp Physiol* 271: R647–R653, 1996.

33. **Franchini KG, Mattson DL, Cowley AW Jr.** Vasopressin modulation of medullary blood flow and pressure-natriuresis-diuresis in the decerebrated rat. *Am J Physiol Regul Integr Comp Physiol* 272: R1472–R1479, 1997.

34. **Garcia-Estãn. J, Roman RJ.** Role of renal interstitial hydrostatic pressure in the pressure diuresis response. *Am J Physiol Renal Fluid Electrolyte Physiol* 256: F63–F70, 1989.

35. **Glabman S, Aynedjian HS, Bank N.** Micropuncture study of the effect of acute reductions in glomerular filtration rate on sodium and water reabsorption by the proximal tubules of the rat. *J Clin Invest* 44: 1410–1416, 1965.

36. **Granger JP.** Pressure natriuresis. Role of renal interstitial hydrostatic pressure. *Hypertension* 19: I9–17, 1992.

37. **Granger JP, Alexander BT, Llinas M.** Mechanisms of pressure natriuresis. *Curr Hypertens Rep* 4: 152–159, 2002.

38. **Guarasci GR, Kline RL.** Pressure natriuresis following acute and chronic inhibition of nitric oxide synthase in rats. *Am J Physiol Regul Integr Comp Physiol* 270: R469–R478, 1996.

39. **Hawk CT, Li L, Schafer JA.** AVP and aldosterone at physiological concentrations have synergistic effects on Na+ transport in rat CCD. *Kidney Int Suppl* 57: S35–S41, 1996.

40. **Holliger C, Lemley KV, Schmitt SL, Thomas FC, Robertson CR, Jamison RL.** Direct determination of vasa recta blood flow in the rat renal papilla. *Circ Res* 53: 401–413, 1983.

41. **Ikenaga H, Suzuki H, Ishii N, Itoh H, Saruta T.** Role of NO on pressurenatriuresis in Wistar-Kyoto and spontaneously hypertensive rats. *Kidney Int* 43: 205–211, 1993.

42. **Inoue T, Nonoguchi H, Tomita K.** Physiological effects of vasopressin and atrial natriuretic peptide in the collecting duct. *Cardiovasc Res* 51: 470–480, 2001.

43. **Jamison RL, Lacy FB.** Effect of saline infusion on superficial and juxtamedullary nephrons in the rat. *Am J Physiol* 221: 690–697, 1971.

44. **Jin C, Hu C, Polichnowski A, Mori T, Skelton M, Ito S, Cowley AW Jr.** Effects of renal perfusion pressure on renal medullary hydrogen peroxide and nitric oxide production. *Hypertension* 53: 1048–1053, 2009.

45. **Kaloyanides GJ, DiBona GF, Raskin P.** Pressure natriuresis in the isolated kidney. *Am J Physiol* 220: 1660–1666, 1971.

46. **Kennedy-Lydon TM, Crawford C, Wildman SS, Peppiatt-Wildman CM.** Renal pericytes: regulators of medullary blood flow. *Acta Physiol (Oxf)* 207: 212–225, 2013.

47. **Khavandi K, Greenstein AS, Sonoyama K, Withers S, Price A, Malik RA, Heagerty AM.** Myogenic tone and small artery remodelling: insight into diabetic nephropathy. *Nephrol Dial Transplant* 24: 361–369, 2009.

48. **Khraibi AA, Knox FG.** Effect of renal decapsulation on renal interstitial hydrostatic pressure and natriuresis. *Am J Physiol Regul Integr Comp Physiol* 257: R44–R48, 1989.

49. **Kim J, Pannabecker TL.** Two-compartment model of inner medullary vasculature supports dual modes of vasopressin-regulated inner medullary blood flow. *Am J Physiol Renal Physiol* 299: F273–F279, 2010.

50. **Knox FG, Schneider EG, Willis LR, Strandhoy JW, Ott CE.** Effect of volume expansion on sodium excretion in the presence and absence of increased delivery from superficial proximal tubules. *J Clin Invest* 52: 1642–1646, 1973.

51. **Kriz W.** Der architektonische und funktioneile Aufbau der Rattenniere. *Cell Tissue Res* 82: 495–535, 1967.

52. **Kunau RT, Lameire NH.** The effect of an acute increase in renal perfusion pressure on sodium transport in the rat kidney. *Circ Res* 39: 689–695, 1976.

53. **Kuschinsky W, Wahl M, Wunderlich P, Thurau K.** Different correlations between plasma protein concentration and proximal fractional reabsorption in the rat during acute and chronic saline infusion. *Pflügers Arch* 321: 102–120, 1970.

54. **Lameire NH, Lifschitz MD, Stein JH.** Heterogeneity of nephron function. *Annu Rev Physiol* 39: 159–184, 1977.

55. **Layton AT, Dantzler WH, Pannabecker TL.** Urine concentrating mechanism: impact of vascular and tubular architecture and a proposed descending limb urea-Na$^+$ cotransporter. *Am J Physiol Renal Physiol* 302: F591–F605, 2012.

56. **Liu KL, Lo M, Grouzmann E, Mutter M, Sassard J.** The subtype 2 of angiotensin II receptors and pressure-natriuresis in adult rat kidneys. *Br J Pharmacol* 126: 826–832, 1999.

57. **Lo M, Liu KL, Clemitson JR, Sassard J, Samani NJ.** Chromosome 1 blood pressure QTL region influences renal function curve and salt sensitivity in SHR. *Physiol Genomics* 8: 15–21, 2002.

58. **Lo M, Liu KL, Lantelme P, Sassard J.** Subtype 2 of angiotensin II receptors controls pressure-natriuresis in rats. *J Clin Invest* 95: 1394–1397, 1995.

59. **Loutzenhiser R, Bidani A, Chilton L.** Renal myogenic response: kinetic attributes and physiological role. *Circ Res* 90: 1316–1324, 2002.

60. **Madrid MI, Garc'ıa-Salom M, Tornel J, Gasparo MD, Fenoy FJ.** Effect of interactions between nitric oxide and angiotensin II on pressure

diuresis and natriuresis. *Am J Physiol Regul Integr Comp Physiol* 273: R1676–R1682, 1997.

61. **Makhanova N, Lee G, Takahashi N, Sequeira Lopez ML, Gomez RA, Kim HS, Smithies O.** Kidney function in mice lacking aldosterone. *Am J Physiol Renal Physiol* 290: F61–F69, 2006.

62. **van der Mark J, Kline RL.** Altered pressure natriuresis in chronic angiotensin II hypertension in rats. *Am J Physiol Regul Integr Comp Physiol* 266: R739–R748, 1994.

63. **Martino JA, Earley LE.** Relationship between intrarenal hydrostatic pressure and hemodynamically induced changes in sodium excretion. *Circ Res* 23: 371–386, 1968.

64. **Masilamani S, Hobbs GR, Baylis C.** The acute pressure natriuresis response blunted and the blood pressure response reset in the normal pregnant rat. *Am J Obstet Gynecol* 179: 486–491, 1998.

65. **Mattson DL, Lu S, Roman RJ, Cowley AW Jr.** Relationship between renal perfusion pressure and blood flow in different regions of the kidney. *Am J Physiol Regul Integr Comp Physiol* 264: R578–R583, 1993.

66. **Mattson DL, Raff H, Roman RJ.** Influence of angiotensin II on pressure natriuresis and renal hemodynamics in volume-expanded rats. *Am J Physiol Regul Integr Comp Physiol* 260: R1200–R1209, 1991.

67. **McDonough AA, Leong PK, Yang LE.** Mechanisms of pressure natriuresis: how blood pressure regulates renal sodium transport. *Ann NY Acad Sci* 986: 669–677, 2003.

68. **Moss R, Thomas SR.** Hormonal regulation of salt and water excretion: a mathematical model of whole-kidney function and pressure-natriuresis. *Am J Physiol Renal Physiol* 306: F224–F248, 2014.

69. **Navar LG, Arendshorst WJ, Pallone TL, Inscho EW, Imig JD, Bell PD.** The renal microcirculation. In: *Comprehensive Physiology*, edited by Terjung RL. New York: John Wiley & Sons, chapt. 13, 2011, p. 550–683.

70. **Navar LG, Bell PD, Burke TJ.** Autoregulatory responses of superficial nephrons and their association with sodium excretion during arterial pressure alterations in the dog. *Circ Res* 41: 487–496, 1977.

71. **Pallone TL, Edwards A, Mattson DL.** Renal medullary circulation. *Compr Physiol* 2: 97–140, 2012.

72. **Pallone TL, Robertson CR, Jamison RL.** Renal medullary microcirculation. *Physiol Rev* 70: 885–920, 1990.

73. **Pannabecker TL, Abbott DE, Dantzler WH.** Three-dimensional functional reconstruction of inner medullary thin limbs of Henle's loop. *Am J Physiol Renal Physiol* 286: F38–F45, 2004.

74. **Patel A, Layne S, Watts D, Kirchner KA.** L-arginine administration normalizes pressure natriuresis in hypertensive Dahl rats. *Hypertension* 22: 863–869, 1993.

75. **Pries AR, Neuhaus D, Gaehtgens P.** Blood viscosity in tube flow: dependence on diameter and hematocrit. *Am J Physiol Heart Circ Physiol* 263: H1770–H1778, 1992.

76. **Pries AR, Secomb TW, Gessner T, Sperandio MB, Gross JF, Gaehtgens P.** Resistance to blood flow in microvessels in vivo. *Circ Res* 75: 904–915, 1994.

77. **Reif MC, Troutman SL, Schafer JA.** Sodium transport by rat cortical collecting tubule. Effects of vasopressin and desoxycorticosterone. *J Clin Invest* 77: 1291–1298, 1986.

78. **Roman RJ.** Abnormal renal hemodynamics and pressure-natriuresis relationship in Dahl salt-sensitive rats. *Am J Physiol Renal Fluid Electrolyte Physiol* 251: F57–F65, 1986.

79. **Roman RJ.** Pressure-diuresis in volume-expanded rats. Tubular reabsorption in superficial and deep nephrons. *Hypertension* 12: 177–183, 1988.

80. **Roman RJ, Cowley AW.** Abnormal pressure-diuresis-natriuresis response in spontaneously hypertensive rats. *Am J Physiol Renal Fluid Electrolyte Physiol* 248: F199–F205, 1985.

81. **Roman RJ, Cowley AW Jr.** Characterization of a new model for the study of pressure-natriuresis in the rat. *Am J Physiol Renal Fluid Electrolyte Physiol* 248: F190–F198, 1985.

82. **Roman RJ, Cowley AW Jr, Garcia-Estãn J, Lombard JH.** Pressure-diuresis in volume-expanded rats. Cortical and medullary hemodynamics. *Hypertension* 12: 168–176, 1988.

83. **Roman RJ, Kaldunski M.** Pressure natriuresis and cortical and papillary blood flow in inbred Dahl rats. *Am J Physiol Regul Integr Comp Physiol* 261: R595–R602, 1991.

84. **Romero JC, Knox FG.** Mechanisms underlying pressure-related natriuresis: the role of the renin-angiotensin and prostaglandin systems state of the art lecture. *Hypertension* 11: 724–738, 1988.

85. **Sadowski J, Dobrowolski L.** The renal medullary interstitium: focus on osmotic hypertonicity. *Clin Exp Pharmacol Physiol* 30: 119–126, 2003.

86. **Sands JM.** Regulation of renal urea transporters. *J Am Soc Nephrol* 10: 635–646, 1999.

87. **Sands JM, Blount MA, Klein JD.** Regulation of renal urea transport by vasopressin. *Trans Am Clin Climatol Assoc* 122: 82–92, 2011.

88. **Sands JM, Knepper MA.** Urea permeability of mammalian inner medullary collecting duct system and papillary surface epithelium. *J Clin Invest* 79: 138- 147, 1987.

89. **Sands JM, Layton HE.** The urine concentrating mechanism and urea transporters. In: *Seldin and Giebisch's The Kidney: Physiology and Pathophysiology* (4th ed), edited by Alpern RJ, Hebert SC. New York: Elsevier, 2008, p. 1143–1178.

90. **Sands JM, Nonoguchi H, Knepper MA.** Vasopressin effects on urea and $H_2O$ transport in inner medullary collecting duct subsegments. *Am J Physiol Renal Fluid Electrolyte Physiol* 253: F823–F832, 1987.

91. **Schmidt-Nielsen B.** Urea excretion in mammals. *Physiol Rev* 38: 139–168, 1958.

92. **Schnermann J, Häberle DA, Davis JM, Thurau K.** Tubuloglomerular feedback control of renal vascular resistance. In: *Handbook of Physiology. Renal Physiology*, edited by Windhager EE. Bethesda, MD: Am Physiol Soc, sect. 8, chapt. 34, 1992, pp. 1675–1705.

93. **Schnermann J, Traynor T, Yang T, Arend L, Huang YG, Smart A, Briggs JP.** Tubuloglomerular feedback: new concepts and developments. *Kidney Int Suppl* 67: S40–S45, 1998.

94. **Selkurt EE, Womack I, Dailey WN.** Mechanism of natriuresis and diuresis during elevated renal arterial pressure. *Am J Physiol* 209: 95–99, 1965.

95. **Sjöquist M, Göransson A, Källskog O, Ulfendahl HR.** The influence of tubulo-glomerular feedback on the autoregulation of filtration rate in superficial and deep glomeruli. *Acta Physiol Scand* 122: 235–242, 1984.

96. **Sonnenberg H.** Renal response to blood volume expansion: distal tubular function and urinary excretion. *Am J Physiol* 223: 916–924, 1972.

97. **Sonnenberg H.** Secretion of salt and water into the medullary collecting duct of Ringer-infused rats. *Am J Physiol* 228: 565–568, 1975.

98. **Sonnenberg H, Honrath U, Wilson DR.** Effects of increased perfusion pressure on medullary collecting duct function. *Can J Physiol Pharmacol* 68: 402–407, 1990.

99. **Strassberg J, Paule J, Gonick HC, Maxwell MH, Kleeman CR.** The quantitative estimation of perfusible glomeruli and the collagen and noncollagen nitrogen of the normal kidney. *Nephron* 4: 384–393, 1967.

100. **Takenaka T, Harrison-Bernard LM, Inscho EW, Carmines PK, Navar LG.** Autoregulation of afferent arteriolar blood flow in juxtamedullary nephrons. *Am J Physiol Renal Fluid Electrolyte Physiol* 267: F879–F887, 1994.

101. **Takezawa K, Cowley AW Jr, Skelton M, Roman RJ.** Atriopeptin III alters renal medullary hemodynamics and the pressure-diuresis response in rats. *Am J Physiol Renal Fluid Electrolyte Physiol* 252: F992–F1002, 1987.

102. **Thomson SC, Blantz RC, Vallon V.** Increased tubular flow induces resetting of tubuloglomerular feedback in euvolemic rats. *Am J Physiol Renal Fluid Electrolyte Physiol* 270: F461–F468, 1996.

103. **Wang CT, Chin SY, Navar LG.** Impairment of pressure-natriuresis and renal autoregulation in ANG II-infused hypertensive rats. *Am J Physiol Renal Physiol* 279: F319–F325, 2000.

104. **Yuan J, Pannabecker TL.** Architecture of inner medullary descending and ascending vasa recta: pathways for countercurrent exchange. *Am J Physiol Renal Physiol* 299: F265–F272, 2010.

105. **Zimmerhackl B, Robertson CR, Jamison RL.** Fluid uptake in the renal papilla by vasa recta estimated by two methods simultaneously. *Am J Physiol Renal Fluid Electrolyte Physiol* 248: F347–F353, 1985.

106. **Zimmerhackl B, Robertson CR, Jamison RL.** The microcirculation of the renal medulla. *Circ Res* 57: 657–667, 1985.